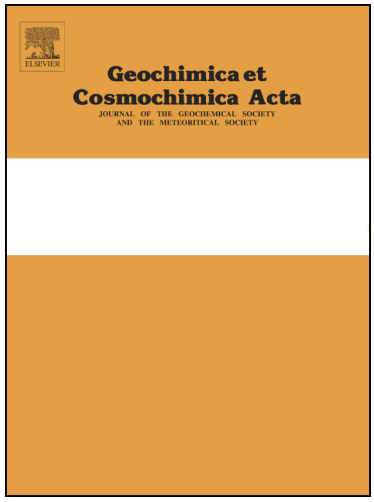

Roles of forest bioproductivity, transpiration and fire in a nine-year record of cave dripwater chemistry from southwest Australia

P.C. Treble, I.J. Fairchild, A. Baker, K.T. Meredith, M.S. Andersen, S.U. Salmon, C. Bradley, P.M. Wynn, Stuart Hankin, A. Wood, E. McGuire

PII: S0016-7037(16)30176-4
DOI: http://dx.doi.org/10.1016/j.gca.2016.04.017
Reference: GCA 9712

To appear in: *Geochimica et Cosmochimica Acta*

Received Date: 13 December 2015
Accepted Date: 8 April 2016

Please cite this article as: Treble, P.C., Fairchild, I.J., Baker, A., Meredith, K.T., Andersen, M.S., Salmon, S.U., Bradley, C., Wynn, P.M., Hankin, S., Wood, A., McGuire, E., Roles of forest bioproductivity, transpiration and fire in a nine-year record of cave dripwater chemistry from southwest Australia, *Geochimica et Cosmochimica Acta* (2016), doi: http://dx.doi.org/10.1016/j.gca.2016.04.017

Roles of forest bioproductivity, transpiration and fire in a nine-year record of cave dripwater chemistry from southwest Australia

[a,b]P.C. Treble*, [c,d]I.J. Fairchild, [b]A. Baker, [a]K.T. Meredith, [b]M.S. Andersen, [e]S.U. Salmon, [c,d]C. Bradley, [f]P.M. Wynn, [a]Stuart Hankin, [g]A. Wood and [g]E. McGuire

[a]Institute for Environmental Research, Australian Nuclear Science and Technology Organisation, Lucas Heights NSW, Australia

[b]Connected Waters Initiative Research Centre, UNSW Australia, Sydney NSW, Australia

[c]School of Geography, Earth and Environmental Sciences, University of Birmingham, Edgbaston, Birmingham, UK

[d]Birmingham Institute for Forest Research, University of Birmingham, Edgbaston, Birmingham, UK

[e]School of Earth and Environment, University of Western Australia, Nedlands WA, Australia

[f]Lancaster Environment Centre, Lancaster University, Lancaster, LA1 4YQ, UK

[g]Department of Parks and Wildlife, Busselton WA, Australia

*Corresponding author:

PMB 2001 Kirrawee DC NSW 2232, Australia

T: +61-2-9717 9356

F: +61-2-9717 3599

E-mail addresses: pauline.treble@ansto.gov.au

Keywords: Golgotha Cave, fire on karst, speleothem, forest bioproductivity, cave dripwater chemistry, mass balance

Abstract

Forest biomass has the potential to significantly impact the chemistry and volume of diffuse recharge to cave dripwater via the processes of nutrient uptake, transpiration and forest fire. Yet to-date, this role has been under-appreciated in the interpretation of speleothem trace element records from forested catchments. In this study, the impact of vegetation is examined and quantified in a long-term monitoring program from Golgotha Cave, SW Australia. The contribution of salts from rain and dry-deposition of aerosols and dissolved elements from soil mineral and bedrock dissolution to dripwater chemistry are also examined. This study is an essential pre-requisite for the future interpretation of trace element data from SW Australian stalagmite records, whose record of past environmental change will include alterations in these biogeochemical fluxes. Solute concentrations in dripwater vary spatially, supporting the existence of distinct flow paths governed by varying amounts of transpiration as well as nutrient uptake by deeply-rooted biomass. Applying principal components analysis, we identify a common pattern of variation in dripwater Cl, Mg, K, Ca, Sr and Si, interpreted as reflecting increasing transpiration, due to forest growth. Mass-balance calculations show that increasing elemental sequestration into biomass has the largest impact on SO_4, providing an explanation for the overall falling dripwater SO_4 concentrations through time, in contrast to the transpiration-driven rising trend dominating other ions. The long-term rise in transpiration and nutrient uptake driven by increased forest bioproductivity and its impact on our dripwater chemistry is attributed to i. the post-fire recovery of the forest understorey after fire impacted the site in 2006 CE; ii. and/or increased water and nutrient demand as trees in the overlying forest mature. The impact of climate-driven changes on the water balance is also examined. Finally, the implications for interpreting SW Australian speleothem trace element records are discussed.

1. INTRODUCTION

Speleothem trace element records serve as proxies for diverse information including recharge (McMillan et al., 2005; McDonald et al., 2004; Johnson et al., 2006; Tremaine and Froelich, 2013), soil and bedrock weathering (Musgrove and Banner, 2004; Hori et al., 2014; Rutlidge et al., 2014), aerosol flux (Frisia et al., 2005), organic matter composition and flux (Hartland et al., 2012) and cave P_{CO_2} (Wynn et al., 2014a; Treble et al., 2015). These records are readily obtained at high resolution (seasonal or better) using laser ablation, secondary ionisation mass spectrometry (SIMS) or synchrotron instruments (Fairchild and Treble, 2009). Such data may reveal annual chemical laminae which are useful for chronological purposes (Treble et al., 2003; Sundqvist et al., 2013; Orland et al., 2014) or to identify seasonal recharge characteristics (Borsato et al., 2007; Fairchild et al., 2010).

Trace elements are thus an excellent complement to stable oxygen and carbon, given their potential to reduce the uncertainties of isotopic records when interpreted in multi-proxy fashion (Fairchild and Treble, 2009). For example, Cruz et al. (2007) and Treble et al. (2003) both draw on trace element data to distinguish meteoric source versus trajectory effects in stalagmite $\delta^{18}O$ records. Speleothem trace element records are also used as paleoenvironmental records in their own right, particularly in situations where the interpretation of stable isotopes might be complicated by mineralogical changes (e.g. McMillan et al., 2005).

Ions in cave dripwater may be derived from incoming meteoric precipitation, dust, sea spray and soil/bedrock leaching (Baker et al., 2000; Fairchild and Treble, 2009; Hartland et al., 2012), although their ultimate concentrations may be dominated by subsequent water/rock interactions occurring along individual water flow paths associated with the hydrological routing (Tooth and Fairchild, 2003; Baldini et al., 2006; McDonald and Drysdale, 2007). Their appeal as proxies lies in their sensitivity to various hydrological and biogeochemical processes, which have been validated via modern speleothem studies. For example, Treble et al. (2003) demonstrated that Mg concentrations in a SW Australian stalagmite clearly responded to a significant decrease in rainfall. In this case, the

mechanism of prior calcite precipitation (PCP) following reduced infiltration was invoked. PCP describes the precipitation of calcite from a solution before it reaches the stalagmite as the fluid equilibrates with lower P_{CO_2} along its flow path in the unsaturated zone (Fairchild et al., 2000). Removal of Ca causes fluid (and hence stalagmite) ion/Ca ratios to rise.

Studies of *vegetation-related* processes have centred on influences of soil PCO_2 or retention of trace elements in the ecosystem-soil environment. Qualitatively, an increase in speleothem $\delta^{13}C$ is commonly attributed to a lowered soil PCO_2 caused by loss of vegetation cover (Fairchild & Frisia, 2014). Seasonal loss of colloid-associated trace elements from soils can be associated with a peak in fluorescent organic matter (Baker et al., 2008) and a multi-year record of these effects, at the forested Alpine site of Grotta di Ernesto, was linked to an historic episode of deforestation (Borsato et al., 2007). Reforestation above a modern mine cavity site in the UK during the 20th century led to a reversal of both $\delta^{13}C$ and trace element signals (Baldini et al., 2005; Fairchild and Hartland, 2010). Progress in quantifying solute storage effects has been made at the Ernesto site where the late 20th century rise in sulphur pollution is lagged and attenuated in dripwater and speleothem records by around 20 years, due to storage in soil and vegetation (Wynn et al., 2013; Borsato et al., 2015). This work was combined with studies of S distribution in wood (Fairchild et al., 2009; Wynn et al., 2014b) to study environmental S loading using trees and speleothems in parallel.

In water-stressed environments such as Western Australia, the potential for transpiration to raise solute concentrations in the vadose zone, hence in dripwater, is expected to be high. This region therefore offers an opportunity to quantify, for the first time, the effects of transpiration as well as uptake of ions as nutrients by vegetation and hence determine the impact of vegetation dynamics on dripwater and speleothem chemistry. Although climatically imposed changes in water balance can be expected to have an impact, there is also the potential that a system in steady-state will be disrupted by fire or by land-use change with implications for dripwater chemistry.

In this paper, more than nine years of cave monitoring data are presented, focusing on chemistry data from five drip sites in the long-term monitoring study at Golgotha Cave, SW Western Australia. The site is situated in a forested catchment and is a well-characterised system (Treble et al., 2013; 2015) with a relatively simple hydrogeology compared to other karst environments providing clearer distinction of hydrogeochemical processes. For example, studies in karst systems where fracture-dominated flow occurs in mature limestones is typically associated with more complex flow dynamics (Baker and Brunsdon, 2003). Principal components analysis (PCA) is used to highlight the main processes influencing dripwater solute concentrations and via a quantitative mass-balance approach the main sources of solutes and changes in their input to the dripwaters are identified. The impact of the deeply-rooted vegetation on solutes in the vadose zone e.g. via transpiration and nutrient uptake is demonstrated. The relative impact of post-fire vegetation re-growth, as well as climate-driven changes in the hydrologic water balance, on our dripwater chemistry, are also examined.

2. SITE DESCRIPTION

2.1 Golgotha Cave location and climate

Golgotha Cave (36.10°S 115.05°E; Fig. 1A) is developed in the Spearwood System of the Tamala Limestone, a coastal belt of dune limestone that extends along >1000 km of the SW Western Australia coastline (Figure 1B). The Spearwood System comprises medium to coarse grained Quaternary aeolian calcarenite mantled by weathered siliceous dune sands (Hall and Marnham, 2002). Golgotha Cave lies in the winter rainfall zone of southern Australia: >75% of annual precipitation falls between May and September. Golgotha Cave is located between a network of Bureau of Meteorology stations, the closest being 7 km away, hence we adopt modelled climate parameters for the cave location from the Australian Water Availability Project (AWAP) dataset (Raupach et al., 2009; 2011). These annual mean values are: precipitation (P) 1113±165 mm, open water pan evaporation (E) 1507±58 mm and actual evapotranspiration (ET) 730±42 mm over the

period 1985-2014. The SW Australian region has experienced decreasing rainfall since ~1970 CE with a particular decline since 2000 CE (Bates et al., 2008). For our cave site, mean P has steadily decreased: 1223±172 (1900-1969), 1157±161 (1970-1999) and 1057±157 (2000-2014) mm.

Open water evaporation is high at this site (P/E=0.7) although estimates of actual evapotranspiration are lower (P/AET=1.5). This is supported by studies on SW Australian forests demonstrating that shading by the mature canopy minimises evaporation (O'Connell and Grove, 1996). However, sap-flow measurements suggest that transpiration by these extensive forests is high: comprising 20-44% of annual rainfall, depending upon forest maturity (MacFarlane et al., 2010). Stable isotopic analyses on the dataset presented here show no evidence of isotopic enrichment when dripwaters and rainfall were compared (Treble et al., 2013) which implies minimal evaporation effects.

Modelled dust flux from inland Australia is small or insignificant, dust in this coastal area being mainly sourced from the surrounding calcareous dunes (Hingston and Gailitis, 1976). However, the prevailing mid-latitude westerly winds ensure a high marine aerosol flux e.g. annual chloride precipitation is >100 kg/ha along the SW Australian coastline (Hingston and Gailitis, 1976).

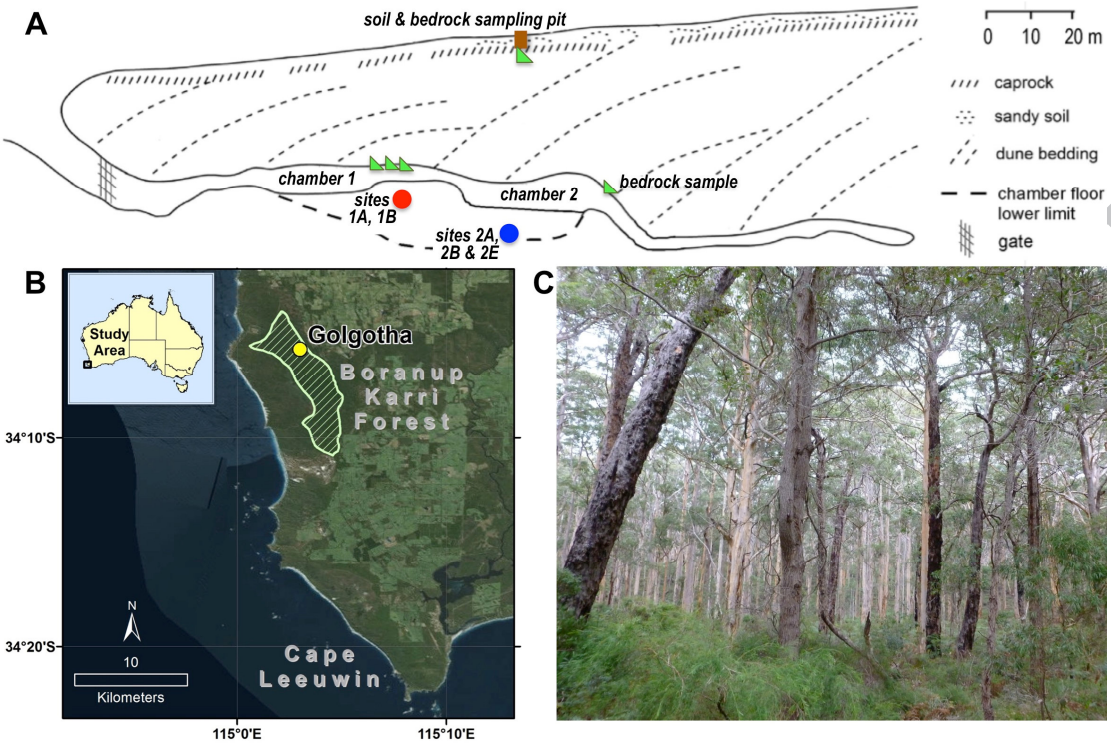

Figure 1A-C: Longitudinal cross section view of Golgotha Cave showing sampling areas (A); the location of Golgotha Cave, southwest Western Australia (B); and photograph of mixed karri-marri forest above Golgotha Cave (C). See Figure 1 in Treble et al. (2015) for plan view of cave. The brown square indicates the location of the soil sampling pit and green triangles indicate the location of bedrock samples collected for this study (see Table 1 for further information).

2.2 Golgotha Cave hydrology

Golgotha Cave is the only long-term continuously monitored cave environment in a highly porous limestone (calcarenite), globally. Our five monitoring sites are located in two chambers of Golgotha Cave (Figure 1A) and the flow path hydrology to these sites has been investigated in a dripwater $\delta^{18}O$ and forward-model study (Treble et al., 2013) and by LiDAR coupled with high temporal and spatial-resolution drip logger studies (Mahmud et al., 2015a; 2015b). The dune facies of the bedrock bounding the two chambers where dripwater is collected contrast markedly in their appearance (Treble et al., 2013). The ceiling over the monitored sites in chamber 1 consists of an Fe-stained and

highly friable horizon (possible paleosol) but is otherwise relatively featureless apart from patches of stalactites. The ceiling of chamber 2 is less weathered in appearance and is less stable than chamber 1, evidenced by roof collapse.

Sites 1A and 1B are situated in the first chamber, 60 m into the cave, while sites 2A, 2B and 2E are in the second chamber, 90 m into the cave (Fig. 1A). Sites 1A and 1B are 0.5 m apart and lie below a circular patch of stalactites receiving matrix-flow, characteristic of the majority of chamber 1 drips (Mahmud et al., 2015a; 2015b). Sites 2A, 2B and 2E are located on a large mound (approximately 6 m radius) of actively forming flowstone and stalagmites in a zone of higher dripwater flux. Site 2E, our highest flowing drip, lies at the centre, and sites 2A and 2B are at the periphery of this mound. Site 2E was classified as combined-flow (matrix plus contributions from fractures and fissures) while sites 2A and 2B were classified as matrix flow by Mahmud et al. (2015b).

Data from the five long-term monitoring sites indicate that drip rates were almost constant at each site over the duration of the study (Treble et al., 2013) despite highly seasonal winter precipitation and a summer soil moisture deficit. This is consistent with matrix flows that are proportional to matrix permeability (Mahmud et al., 2015b). However, there were three periods of typically higher drip rates, indicating recharge, coinciding with above average rainfall in 2005, 2008-2009 and 2013 CE described in Treble et al. (2013) and (Mahmud et al., 2015b). The increase in drip rate due to increased discharge is relatively instantaneous, indicative of activation of piston-flow (Treble et al., 2013).

It has not been possible to constrain the residence times of vadose zone water from infiltration to dripwater with certainty at this stage of the project. However, measurements of tritium in these dripwaters during August 2010 ranged from 1.3±0.1 to 1.7±0.2 TU (average: 1.5 TU, n=5) are generally within error of the lower limit of rainfall weighted ^{3}H values in Perth rainfall from 2005-

2011 (1.6-2.0 TU) (Tadros et al., 2014). Treble et al. (2013) suggested a 6-9 month transit time based on the lag between quasi-seasonal cycles observed in rainfall and similar (attenuated) cycles in dripwater $\delta^{18}O$.

2.3 Vegetation and catchment fire history

Golgotha Cave is located within the Leeuwin-Naturaliste National Park and surface vegetation overlying our site (Figure 1C) is a mixed canopy of marri/karri wet eucalypt forest (*Corymbia calophylla,* syn. *Eucalyptus calophylla* and *Eucalyptus diversicolor)* with canopy height of 20-40 m, with a dense understorey of *Agonis flexuosa, Trymalium spathulatum, Xanthorrhoea preissii, Bossiaea disticha* and *Templetonia retusa*; that can reach up to 10 m high. The vegetation root systems are considerably deep in this system and tree roots appeared in the ceiling of chamber 1 in in 2012 CE, penetrating over 25 m of bedrock.

A burn occurred on and around Golgotha Cave early in 2006 (between late February and mid-April), approximately six months after our monitoring commenced. Figure 2A shows the extent of this fire within the immediate catchment of Golgotha Cave and its surrounding area. The differential normalized burn ratio (dNBR; Key and Benson, 2006) was calculated from Landsat TMS imagery for this and two earlier fires (1992 and 1998) as a measure of the relative impact on the forest (Figures 2A-C). The dNBR is an index number between -1 and +1 comparing the ratio of Landsat TMS Band 4 and Band 7 data from two images, one preceding and one following the fire. A positive dNBR is attributed to a greater burn severity, whereas a negative dNBR suggests increased vegetative productivity, and zero indicates no change. The 2006 fire achieved an overall reduction in understorey density (i.e. reduced fuel load), but the effects were spatially highly heterogeneous directly above the cave. The impact of the fire was much greater just to the north and within the catchment of Golgotha Cave (Figure 2A). The earlier wildfire in 1998 was a minor understory fire to the east of the cave, outside of the cave catchment and not visible to satellite (Fig. 2C); presumably

the 1998 fire had little direct impact on the vegetation above the cave. The 1992 fire impacted vegetation the most, both within and surrounding the cave catchment (Figures 2B-C).

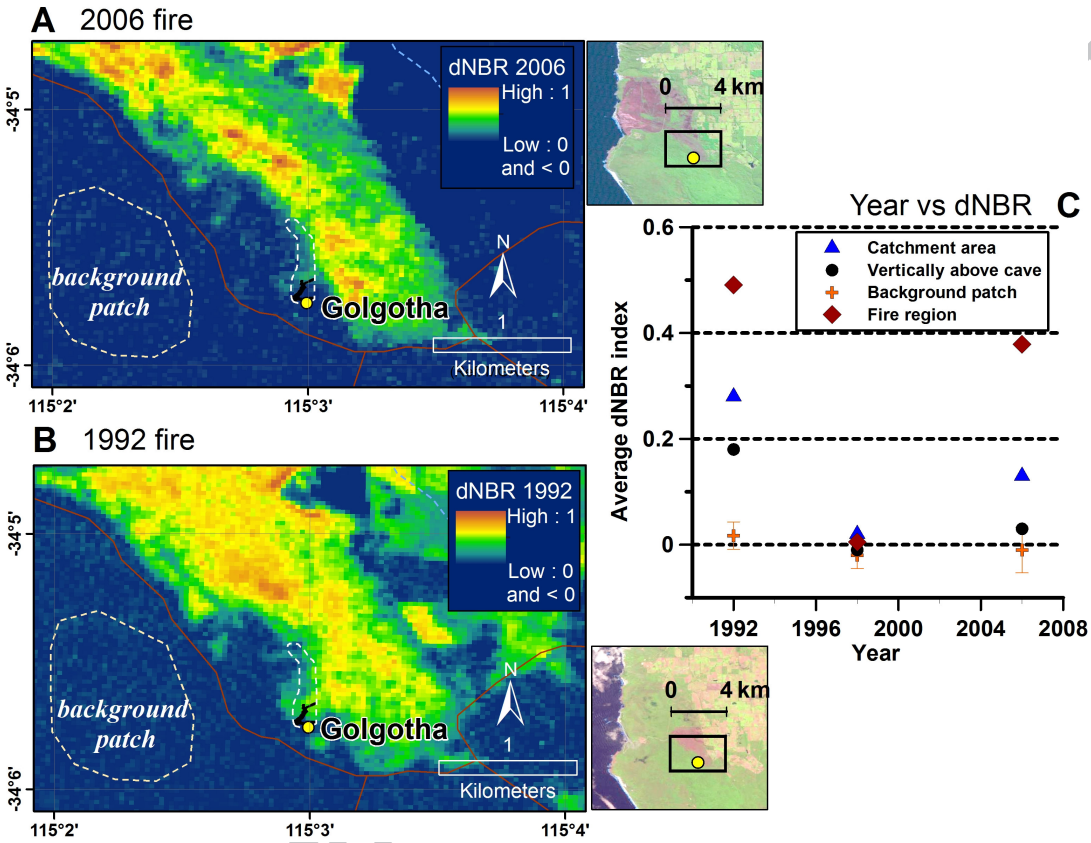

Figure 2A-C: Differential normalised burn ratio (dNBR) image created using Landsat 5 TM data pre-fire (28/2/2006) and post-fire (12/5/2006) (A); pre-fire (4/11/1992) and post-fire (6/12/1992) (B); and average dNBR index per pixel calculated for the larger catchment area for the cave, the area directly above the cave, an unburned background patch and the wider regional fire extent limited to Boranup Karri Forest (see Fig. 1B) for fires in 1992, 1998 and 2006 (C). Location of Golgotha Cave entrance is indicated by yellow dot and black line is the main passageway; white dashed line is the catchment area for Golgotha Cave. The catchment area was calculated by GIS analysis of digital elevation model data (Farr et al., 2007; Gallant et al., 2011). Insets shows the full extent of the larger 1800 Ha 2006 fire, indicated by brown colour, using the post-fire Landsat 5 TM imagery with Bands 3-2-1.

In a previous paper, Treble et al. (2015) reverse-modelled the carbonate parameters in this dataset revealing rising CO_2 source production in the unsaturated zone. This was attributed to increasing bioproductivity which was linked to forest recovery after the 2006 fire (Section 2.2). The values for modelled source CO_2 were also found to be higher than shallow (<0.5 m) measurements of soil CO_2 implying that the dripwaters are receiving a relatively deep source of CO_2 consistent with tree roots injecting CO_2 into the unsaturated zone at depth.

3. Methods

3.1 Bedrock and soil analyses

Five bedrock and seven soil samples were collected (see Fig. 1 for locations and Table 1 for depth information and further description) to determine water-soluble salts as well as bulk composition by acid digestion. Bedrock and soil samples were prepared by passing material through a 2 mm sieve to remove the coarse fraction and crushing approximately 7.5 g of material in a ring grinder. From this, 2 g of crushed powders were rinsed successively three times in MilliQ water (ratio 1:10 by volume) to dissolve water-soluble salts. Rinsing times were approximately 15 minutes. Cation and anion concentrations of the leachates were measured using a Thermo Fisher inductively coupled plasma-atomic emission spectroscopy (ICP-AES) ICAP7600 and a Dionex DX-600 ion chromatograph (IC) with self-regenerating suppressor at ANSTO. Further, dried samples (0.2 g) were digested in a solution of 3 ml HNO_3, 1 ml HCl (Merck Suprapur acids) and 3 ml MilliQ in a laboratory microwave at 180°C for 15 mins. The aqueous solution was diluted to 30 ml and cations were measured by ICP-AES.

3.2 Dripwater and rainwater analyses

Cave dripwaters were sub-sampled from 1 L high-density polyethylene (HDPE) collection vessels at the five sites in Figure 1A between August 2005 and January 2015 at 4-6 week intervals. The collection apparatus as well as other parameters (pH, alkalinity) measured during these visits are detailed in Treble et al. (2015). Five 24 hr rainwater samples (100 ml) were collected from a similar

apparatus as the ones used for dripwaters between 14/5/08 and 9/6/08. Dripwater and rainwater samples were filtered using 0.45 µm mixed-cellulose filters into two 50 ml polypropylene bottles and refrigerated until analysis. One bottle was acidified to 2% HNO_3 in the collection bottle and analysed for cations by ICP-AES and anions were determined on the other sub-sample by IC at ANSTO. An internal standard with concentrations approximating the cave waters was included in each cation batch to check between-run reproducibility. Saturation indices for dripwater PCO_2 (Treble et al., 2015) and other minerals were calculated using the WATEQ4F thermodynamic database in PHREEQC 2.4.2 program (Parkhurst and Appelo, 1999) to assess possible precipitation/dissolution reactions. Charge balance errors were checked for samples with a full suite of major ion chemistry and 89% of our data were within ±5% and the remaining were within ±10%.

As previously noted (Treble et al., 2015), seven samples at site 1A had K concentrations between 4 and 450 times higher than the mean. These anomalously high samples coincided with a period when micro-pH electrodes were being used at this site (May 2009 and January 2010) suggesting that the samples had been contaminated by KCl from electrode storage solution. Hence, these K data were discarded and the affected Cl data were corrected by subtracting the calculated contribution of Cl from the KCl, assuming that the K in the affected data were overwhelmingly due to contamination.

Drip rate data are manual measurements (Treble et al., 2013) with the exception of the last 5 points (July 2014 onwards), which are based on automatic drip logger measurements (Mahmud et al., 2015b) calculated over the 24-hour interval coinciding with the cave visits.

3.3 Sulphate isotopes

Dual isotopes of sulphate ($\delta^{34}S\text{-}SO_4$ and $\delta^{18}O\text{-}SO_4$) were measured to assess potential biogeochemical transformations of SO_4 in these dripwaters. Dripwater was collected between 28/05/14 and 09/06/14 from the four of the monitored drip sites and samples were transferred to clean 100 ml

polypropylene bottles. Five rainwater samples were collected between 9/6/14 and 19/6/14 and combined to obtain sufficient sulphate for isotopic analysis. The rain gauge is described in Treble et al. (2013).

Isotopic analyses were conducted primarily following the method of Wynn et al. (2013). Water samples were filtered (0.45 µm cellulose nitrate membrane filters) and loaded onto an AG2-X8 anion exchange resin to extract the sulphate anions. Anions were removed from the AG2-X8 resin using aliquots of 1M ultrapure HCl and sulphate precipitated as barium sulphate following the addition of $BaCl_2$. The barium sulphate precipitate was separated by centrifugation and washed repeatedly with de-ionised water prior to drying and analysis by mass spectrometry. $^{34}S/^{32}S$ and $^{18}O/^{16}O$ ratios of the barium sulphate were determined using a pyrocube elemental analyser linked to an Isoprime 100 mass spectrometer at Lancaster University, UK. Combustion of samples within tin capsules at 1030°C yielded SO_2 for analysis of $\delta^{34}S\text{-}SO_4$ and pyrolysis within silver capsules in the presence of carbon black at 1400°C yielded CO for determination of $\delta^{18}O\text{-}SO_4$. Values were corrected against V-CDT using within run analyses of international standards NBS-127 and SO5. Precision based on replicate analyses of in-house standards was better than 0.3‰ (1SD) for both sulphur and oxygen isotope ratios.

3.4. Principal Components Analysis (PCA) on dripwater

PCA, here performed using XLSTAT® on measurements of solutes and PCO_2, is a multi-dimensional correlation analysis which has been used previously in speleothem studies by, for example, Borsato et al. (2007) and Fairchild et al. (2010). It identifies the main modes of variability of normalized data, expressing these as the first, second, ... nth principal components (PC1, PC2,…, PCn) of variation which contribute successively smaller amounts to the total data variance. Loadings of individual parameters on each PC can be compared qualitatively, but there is no simple way of assessing statistical significance. PCA analysis can only be made where there is complete set of determinands

so sampling dates with an incomplete set of parameters were excluded, especially early in the sampling regime when Si was often below detection. The PCA was repeated using ion/Cl ratios as described in Section 5.1 and Electronic Annexe A.

4. RESULTS

4.1 Soil and bedrock chemistry

Acid digestion of bedrock samples yields the characteristic composition expected of relatively pure carbonate with two exceptions (Table 1). Two of the bedrock samples from site 1 (SWrock0614_8 and SWrock0913_1) had particularly low Ca and relatively higher Si concentrations, consistent with their appearance as more highly weathered material (Section 2.2). Strontium is also higher for these two samples.

Sodium, K, Cl and SO_4 were typically present in the aqueous leachate (Table 1), representing soluble components within fluid inclusions in carbonate minerals or loosely adsorbed or precipitated on mineral surfaces. The patterns of ion distribution in leaches were similar between soil and bedrock samples but concentrations of highly soluble ions were typically higher in the soil samples. Nevertheless mass yields were low: an average of 218 mg/kg, corresponding to <0.1% of total solid leached.

Sodium and Cl are present in all soil leachates and are highest in the shallowest soil (equivalent to 1 mmol of NaCl per kg soil). This is likely to represent soluble salts in the soil caused by complete evaporation of soil water near the surface. The experimental 1:10 solid:fluid ratio used here is similar to the minimum fluid needed to flush a soil, implying that soil water NaCl concentrations may approach 0.1 mmol/l although this would represent a maximum value achievable in nature as the soils were crushed in our experiment, permitting more leaching (McGillen & Fairchild, 2005).

Table 1: Summary of leachate concentration data for crushed bedrock and soil samples, as well as bulk composition determined by acid digestion. Units are mg per kg of solid. Anion data were only obtained for leachates hence elemental S values are reported for bulk composition rather than SO_4. Values for cave chamber 1 bulk and chamber 2 bulk (bold italics) are used to estimate bedrock contribution in mass balance calculations (Section 5.2, equation 5).

Sample code	Description and depth	Ca mg/kg	Mg mg/kg	Na mg/kg	K mg/kg	Sr mg/kg	S mg/kg	Si mg/kg	Cl mg/kg	SO_4 mg/kg
BEDROCK										
Leachate data										
SWrock0913_2	Site 1 ceiling	138	8.4	2.7	2.4	0.74		2.7	24	37
SWrock0614_8	Site 1 ceiling, weathered	158	11	29	11	2.0		8.9	5.7	6.3
SWrock0913_1	Site 1 ceiling, weathered	128	7.1	26	14	1.6		4.9	30	65
SWrock_N11	Clast in 0.8-1.0 m soil depth above site 2	136	6.9	1.2	1.6	0.83		1.9	1.5	2.9
SWrock0913_4	Site 2 ceiling	130	4.5	1.3	2.4	0.72		2.8	4.1	1.8
Bulk composition										
SWrock0913_2	As above	352000	2470	111	134	303	40.8	482		
SWrock0614_8	As above	235000	1390	301	203	815	205	1650		
SWrock0913_1	As above	178000	762	209	178	550	105	1210		
Chamber 1 bulk (n=3)		***255000***	***1541***	***207***	***172***	***556***	***117***	***1114***		
SWrock_N11	As above	372000	2200	66	77.8	361	16.8	255		
SWrock0913_4	As above	354000	1310	47	98	297	<20	400		
Chamber 2 bulk (n=2)		***363000***	***1755***	***57***	***88***	***329***	***17***	***328***		
SOIL										
Leachate data										
SWsoil_N5	Pit 2, 0.1 m	45	*19*	*57*	*47*	*0.14*		*1.6*	44	15
SWsoil_N6	Pit 2, 0.2 m	4.5	2.9	24	30	0.04		7.2	27	4.1
SWsoil_N9	Pit 2, 0.4 m	3.2	1.3	14	4.2	0.02		2.1	7.9	4.5
SWsoil_N4	Pit 2, 0.6 m	12	2.3	13	44	0.09		7.0	8.6	4.1
SWsoil_N7	Pit 2, 1 m	2.7	0.88	9.7	23	0.04		5.0	4.6	6.6
SWsoil_N8	Pit 2, 1.4 m	6.5	1.2	8.9	23	0.08		4.2	5.6	5.1
SWsoil_N1	Pit 1A, 1.7 m	3.6	0.53	9.7	37	0.08		2.1	3.3	2.6

Bulk composition								
SWsoil_N5	As above	640	128	50.9	475	61.3	46	1390
SWsoil_N6	As above	615	164	63.2	530	49.6	71	1290
SWsoil_N9	As above	2990	387	32.5	147	42.7	241	1050
SWsoil_N4	As above	261	87.5	43.3	433	135	21	1370
SWsoil_N7	As above	355	107	34.7	290	64.6	33	1290
SWsoil_N8	As above	302	89.1	37.4	274	104	24	841
SWsoil_N1	As above	261	87.5	43.3	433	135	21	1440

4.2 Dripwater and rainwater chemistry

Dripwater discharge and chemistry at each monitored drip site are summarised in Table 2. Comparing the sites, the range in median values of the main parameters and ions in dripwater are: Ca = 43-75 mg/l, Mg = 7.0-7.8 mg/l; Na = 53-77 mg/l; Cl = 98-159 mg/l and SO_4 = 8.0-12 mg/l. Dripwater Ca is highest for site 2E and attributed to the relatively lower impact of PCP at the stalactite tip at this faster dripping site (Treble et al., 2015). Other ions show no overall relationship with discharge (Table 2). There are some broad spatial relationships in that K and SO_4 are lower, while Sr and Si are higher, in cave chamber 1 versus chamber 2; although there is higher variability between sites in chamber 2. Overall, Na and Cl concentrations increase in the order: 2A<1A≤1B<2E<2B, whilst K and SO_4 concentrations decrease in this order.

Figure 3 shows the time series of monthly precipitation minus actual evapotranspiration (P-AET), cumulative P-AET, drip rate, Cl, Na, K, Mg, Si, Sr, SO_4 and Ca concentrations. The three periods of higher recharge (Section 2.2) are indicated by roman numerals I-III and shaded bars. The impact of PCP is evident in the seasonal variations in Ca at the low-flow sites, as discussed by Treble et al. (2015) but other ions do not show clear seasonality except for Mg at site 2B.

Table 2: Summary of dripwater and rainwater chemistry between August 2005 and January 2015. Drip rate (Treble et al., 2013) is converted to discharge assuming a drip volume of 0.2 ml (Collister and Mattey, 2008).

	Chamber 1				Chamber 2						Rainwater	
	Site 1A		Site 1B		Site 2A		Site 2B		Site 2E			
	median	SD	median	SD	median	SD	median	SD	median	SD	mean	SD
Discharge (ml/day)	63	4.7	40	2.0	47	10	67	85	524	45		
Ca (mg/l)	48	9.0	44	10	44	10	49	11	75	7.7	3.1	1.4
Mg (mg/l)	7.1	0.64	7.2	0.81	7.8	0.49	8.0	0.85	7.6	0.44	1.6	0.71
Na (mg/l)	64	5.5	65	7.6	53	4.0	77	6.6	77	3.3	12	4.6
K (mg/l)	0.92	0.15	0.92	0.22	1.5	0.20	1.5	0.25	1.5	0.17	1.8	1.0
Sr (mg/l)	0.21	0.016	0.21	0.019	0.18	0.010	0.19	0.024	0.19	0.011	0.016	0.0062
Cl (mg/l)	119	6.5	121	8.9	98	8.0	159	8.6	146	5.9	21	9.0
SO_4 (mg/l)	8.0	0.43	8.0	0.53	12	0.73	9.5	0.65	8.2	0.44	3.1	1.3
Si (mg/l)	1.7	0.14	1.6	0.21	1.4	0.13	1.5	0.19	1.4	0.22		
n	85		82		77		84		51		5	

Most ions are characterised by smooth, long-term trends which typically rise over time. The rising trend is clear at all dripwater sites for Cl, albeit varying in magnitude (25% at site 2B versus ~16-18% at other sites) overall, and there is inter-annual variability in Cl concentrations between sites. Although Cl is assumed to be the most conservative ion in our dataset, there are no simple relationships between Cl, infiltration and cave discharge.

Overall, dripwater Cl concentrations are relatively high across all sites, being 5-8 times more concentrated than rainwater (Table 2). Dry aerosol deposition is significant at this coastal site: ~100 kg/ha/a (Hingston and Galitis, 1976) which is equivalent to 16 mg/l assuming a P-AET of 600 mm/a; but this would only account for 10-15% of our dripwater Cl concentrations. The site has a high potential for evaporation (Section 2.1). However, partial evaporation of infiltrating water would lead

to ^{18}O-enrichment in the remaining water which would be evident in the dripwater data (Cuthbert et al., 2014). Such enrichment was not observed for the site (Treble et al., 2013) suggesting that transpiration, which does not lead to ^{18}O-enrichment (Farquhar et al., 2007), rather than evaporation is responsible for these high Cl concentrations. The significant role of transpiration, resulting in high dripwater Cl concentrations, is consistent with the extensive, and deeply rooted, biomass above our cave site.

Dripwater Na, K and Mg show long-term rising trends (Fig. 3) but as per the reasoning above, the overall rise in the concentrations of these ions is too large to be attributed to a rise in dry aerosol deposition. For example, based on the calculations above and the Mg/Cl ratio of seawater, sea salt deposition would have to rise by 200-300% to account for the 25% rise in dripwater Mg concentrations. Rather, transpiration could raise concentrations of these and other ions (e.g. Sr and Si) in the vadose-zone water via ion exclusion (Appelo and Postma, 2007, p. 51). In contrast to all other solutes, dripwater SO_4 actually declines (Fig. 3).

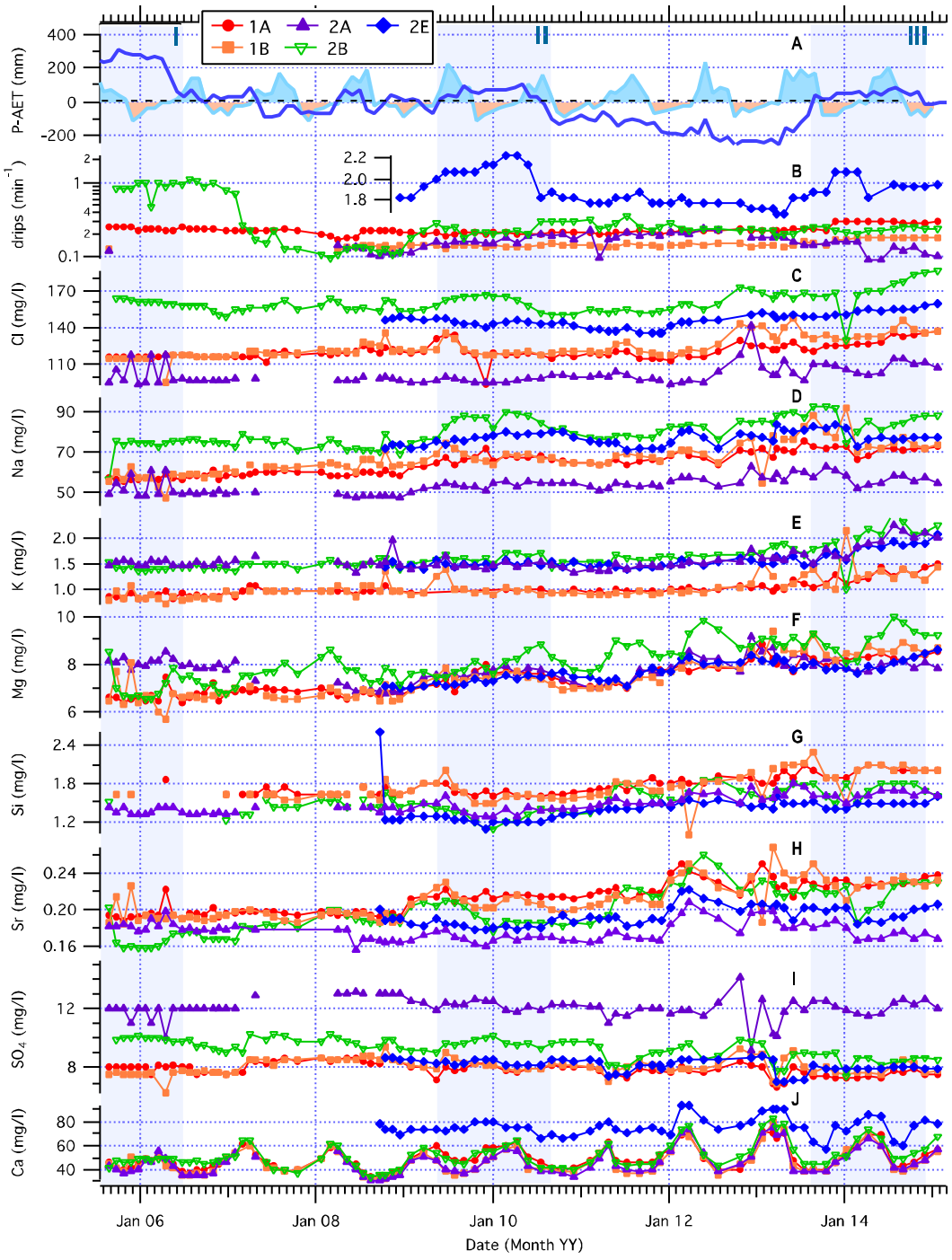

Figure 3: Time series of P-AET (shaded), cumulative P-AET (blue line) (A), drip rate (B), Cl, Na, K, Mg, Si, Sr, SO_4 and Ca (C-J) data at each of the drip sites for Golgotha Cave. Monthly P-AET is calculated using precipitation minus modelled actual evapotranspiration (parameter 'FWE') extracted at our location from the AWAP database (Raupach et al., 2009; 2011). Cumulative P-AET or "residual mass curve" following Hurst (1951) is calculated as the cumulative sum of the monthly P-AET anomaly. The three vertical blue bars,

labelled I-III, indicate periods of higher cumulative P-AET coinciding with increased drip rates at some sites indicating enhanced recharge.

Strontium concentrations are higher and relatively more variable during the period of lowest cumulative P-AET (2012 to mid-2013) and this is apparent at all sites. Dripwater Si shows some broad relationship to cumulative P-AET with concentrations rising at all sites during the period of falling cumulative P-AET (Fig. 3). These observations indicate that our dripwaters comprise a mixed-signal i.e. multiple physical and chemical processes affect the dripwater chemistry. We identify the main processes in the following discussion, by first conducting a Principal Components Analysis (PCA) (Section 5.1) and secondly, by utilising this information to quantify the impact of these processes via mass balance (Section 5.2 and 5.3).

4.3 Sulphate isotopes

Sulphate isotopic results are shown in Table 3. The composite rainfall sample has a $\delta^{34}S\text{-}SO_4$ value of +17.8 ‰ and a $\delta^{18}O\text{-}SO_4$ value of +8.47‰. Both values are close to the isotopic end member values expected from marine aerosols (seawater $\delta^{34}S\text{-}SO_4$ =+21‰ (Rees et al., 1978 and $\delta^{18}O\text{-}SO_4$ =+9.7‰; Lloyd et al., 1967), albeit slightly depleted in both. The depleted nature of the precipitation likely reflects a contribution from alternative sources to the total atmospheric sulphur load e.g. marine biogenic, anthropogenic and non-marine biogenic (Calhoun et al., 1991; Wynn et al., 2008). Dripwater isotopic ratios are close to those of the rainfall sample although mean $\delta^{34}S\text{-}SO_4$ (+19.8‰) is 2‰ higher and mean $\delta^{18}O\text{-}SO_4$ (+5.6‰) is 3‰ lower than rainfall. The higher $\delta^{34}S\text{-}SO_4$ in dripwater relative to rainfall is consistent with a net assimilation of sulphur into the surrounding vegetation (fractionation during assimilation is estimated at 1-2‰), thereby leaving the residual soil solution correspondingly enriched in ^{34}S (e.g. Krouse et al., 1991; Zhang et al., 1998). With regards to $\delta^{18}O\text{-}SO_4$ data, the relative depletion compared with rainwater suggests some re-setting of the O isotope composition of the sulphate, consistent with mineralisation during cycling through the vegetation.

Table 3: List of samples analysed for sulphate isotopes. Dash indicates insufficient sample for analysis.

Sample ID	Description	$\delta^{34}S\text{-}SO_4$	$\delta^{18}O\text{-}SO_4$
Australia 06-2014	rainwater	17.8	8.5
SW1A-140609	dripwater (1A)	20.2	4.9
SW1B-140609	dripwater (1B)	20.0	-
SW2B-140609	dripwater (2B)	19.4	-
SW2E-140609	dripwater (2E)	19.8	6.2

5. DISCUSSION

5.1 Principal Components Analysis (PCA)

PCA was performed initially on the chemical time series of each drip site separately, using eight ions and PCO_2 as parameters, but since similar results were obtained, the analysis was repeated using all data combined. The first three PCs explained 81% of the total variance and the loading of each parameter is illustrated in Table 4, whilst the temporal variation in each PC is shown in Figure 4. PCA was also run on ion/Cl ratios and results are given in Electronic Annex A.

The PCA supports the qualitative data description given above with reference to Figure 3. PC1 explains 38% of the total variance and reflects the long-term trend through the dataset including some of the seasonal variability. Most parameters load positively onto PC1, in the order Na>Cl>Sr>Mg>Ca while SO_4 loads negatively (Table 4). The strength of PC1 increases during the late summer and autumn (i.e. January to May) of each year, as well as after 2010 (Figure 4). This behaviour is common across all sites but the lower scores for site 2A (Fig. 4) suggests that the process implicated in PC1 has less impact at site 2A, consistent with relatively lower Na and Cl concentrations at site 2A, as observed in the data (Section 4.2).

Table 4. Results of PCA on the entire dataset (n = 308): numbers indicate positive or negative loading (analogous to a correlation coefficient) of each parameter on each principal component. The bottom row gives the total percentage of variation in the data explained by each component.

	PC1	PC2	PC3
$logPCO_2$	0.21	-0.02	0.80
Ca	0.51	0.36	0.59
Mg	0.61	0.32	-0.51
Na	0.89	0.22	0.00
Sr	0.77	-0.51	-0.19
SO_4	-0.73	0.48	-0.30
K	0.16	0.89	-0.30
Cl	0.80	0.36	-0.02
Si	0.40	-0.67	-0.42
% explained	38.2	23.8	18.2

The relationship between PC1 and cumulative P-AET is not straightforward. While both exhibit a long-term trend towards the higher concentrations of most ions, there is no clear dilution response to the three recharge events (I-III) described in Section 2.2. For example, PC1 continues to rise towards higher loadings despite the 2013 recharge event, although perhaps less steeply than before. Given 1) the important role of transpiration in controlling Cl concentrations noted in Section 4.2; 2) the high loading of Cl on PC1; and 3), the dry-season maxima, the inference is that PC1 equates broadly with vegetation processes. The negative loading of SO_4 on PC1 implies that the higher the amount of transpiration (which increases Cl and other ions) the greater the removal of SO_4 from water, which is likely to be a biomass assimilation process. Nevertheless, the importance of transpiration in explaining the data is illustrated by the fact that when the PCA is repeated using

ratios of ions to Cl data (i.e. data that are normalised to Cl to adjust for transpiration), the equivalent PC is no longer the leading PC and only explains 20% of data variation (see Electronic Annex A).

PC2 explains 24% of the total variance and Sr and Si load negatively, while SO_4 and K load positively. The main feature of the data represented by PC2 is their spatial variability since chamber 1 sites have quite different values from chamber 2 sites (Figure 4). This reflects differences in the mean concentrations of these ions consistent with higher Sr and Si concentrations measured in chamber 1 versus chamber 2 bedrock composition (Table 1). However, there is also a parallel variation over time in PC2 at all sites, implying the operation of a temporally variable process in which variations of Sr and Si oppose those of K and SO_4. PC2 responds to the second and third recharge periods with more strongly positive values from winter 2009 to winter 2010 and from winter 2013 onwards, suggesting that variations in PC2 represent a process related to the cumulative P-AET (Fig. 4). This is also evident by Pearson Product correlations with higher correlations (r^2=0.2 to 0.4; excluding site 2A) between PC2 and cumulative P-AET, versus lower or no correlation (r^2= 0 to -0.2) between PC1 and cumulative P-AET. Cross-plots of these parameters are provided in Electronic Annex A. The stronger relationship between PC2 and cumulative P-AET suggests that PC2 represents interactions governed by water residence time. Periods of higher cumulative P-AET would represent periods of lower water-rock interaction times, resulting in lower Sr and Si concentrations in the dripwater. Less plant uptake of SO_4 and K during periods of higher water excess may also be expected, consistent with these results for PC2.

PC3 explains 18% of the total variance and is dominated by a seasonal signal with higher loadings in the warmest months from December to April, as well as a trend to higher loadings from 2013 onwards. Dripwater P_{CO_2} and Ca have high positive loadings onto PC3. Given the strong relationship between Ca, P_{CO_2} and PC3, as well as the higher loadings during the cave ventilation season, PC3 clearly represents the influence of carbonate chemistry reactions on our data, especially PCP (Treble

et al., 2015). Other principal components in our combined analysis explain 10% or less of the total variance (Electronic Annex A) and are not considered here.

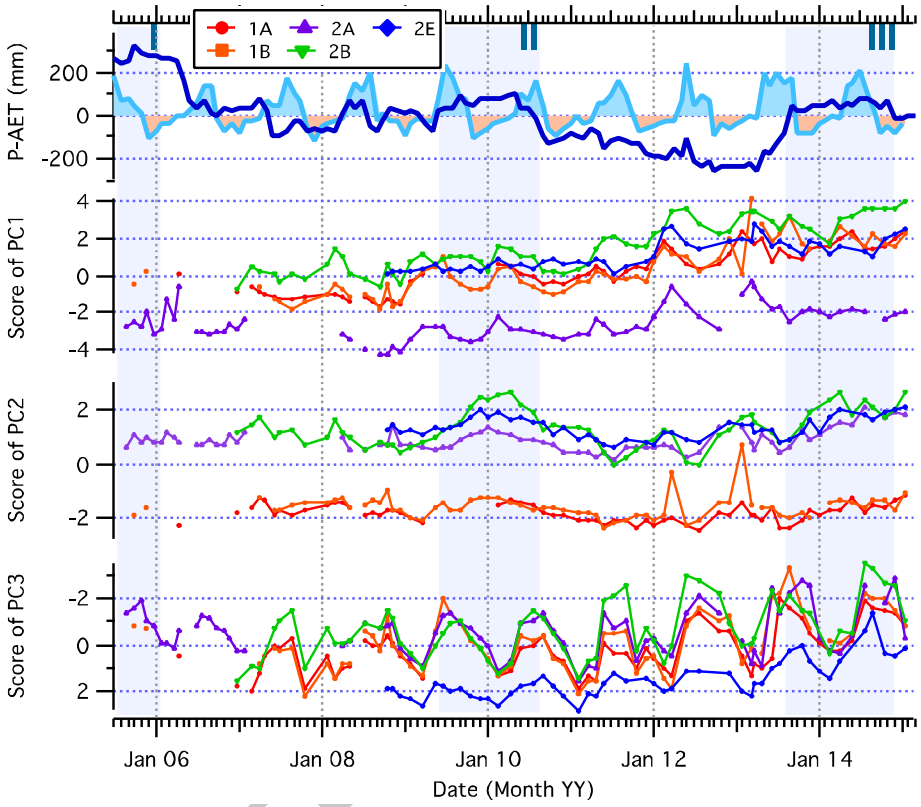

Figure 4: Time series of P-AET (shaded), cumulative P-AET (blue line) (A) and the scores of the principal components: PC1 (B), PC2 (C) and PC3 (D); of dripwater Ca, Mg, Na, K, Si, Cl, SO_4 and PCO_2. The three vertical blue bars, labelled I-III, indicate periods of higher cumulative P-AET coinciding with increased drip rates at some sites indicating enhanced recharge.

The PCA identified statistical relationships in the data and this has assisted in identifying 3 main processes: (1) transpiration and assimilation; (2) water-rock interactions governed by contact time; and (3) PCP. It has indicated that these processes impact individual sites differently e.g. the relative reduced impact of (1) on site 2A and the role of (2) between the two chambers. The analysis also highlights some as yet unexplained processes in that recharge intervals provoke an opposite response in some ions: less Si and Sr, but more K and SO_4, in dripwater. Additionally, the negative

relationship between PC1 (transpiration) and dripwater SO_4 warrants further investigation. In particular, it is important to quantify the sources and sinks of dissolved solutes, and determine how the proportions of these may change through time. In Section 5.2, a mass balance is constructed to address this.

5.2 Mass balance model

The site description and data presented above allow us to construct a conceptual box model of Golgotha Cave hydrology and hydrochemistry which describes both water and elemental fluxes between potential sources and sinks (Figure 5). The sources and processes that we can constrain are marine aerosol input and bedrock contributions (Table 1), and PCP (Treble et al., 2015); while the processes that we cannot constrain in the current study are lumped and described by a residual term (Figure 5). Since Golgotha Cave lies in an unpolluted region, the soluble dust will be largely of similar origin to the local karst bedrock, the dust dissolution component is not treated separately in our mass balance, but is subsumed within bedrock dissolution.

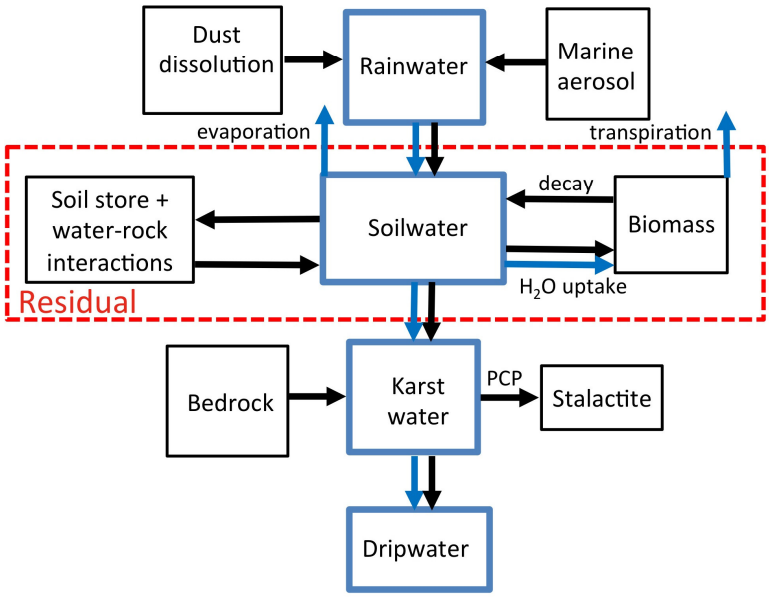

Figure 5. Box model to illustrate mass balance approach to modelling Golgotha dripwater hydrochemistry. Blue arrows indicate water flux and black arrows indicate elemental fluxes. The mass balance used is summarised at the bottom of the diagram; pollution and dust dissolution flux is minor and subsumed under bedrock dissolution.

The mass balance calculations (using Mg as an example) are outlined in the equations below. Aerosol contribution is estimated using the known fixed ion/Cl ratios in seawater (Chester, 1990) and the dripwater Cl concentration:

$$[Mg]_{marine\ aerosol} = [Cl]_{dripwater} \times [Mg/Cl]_{seawater} \quad [1]$$

The impact of PCP is corrected for in equations 2-5. To estimate the initial concentration of Ca, $[Ca]_{initial}$, in the 'Karst Water' store in Fig. 5, we assumed that dripwaters prior to any PCP had a Mg/Ca ratio at least as low as the lowest measured ratio for each site (e.g. 0.111 for site 1A; Treble et al., 2015):

$$[Ca]_{initial} = [Mg]_{dripwater}/0.111 \quad [2]$$

The amount of Ca lost to PCP is: $Ca_{PCP}=[Ca]_{initial} – [Ca]_{dripwater}$ [3]

The small amount of Mg and Sr lost to PCP was calculated using partition coefficients, K_{Mg} = 0.019 for Mg (Huang and Fairchild, 2001) and K_{Sr} = 0.1, the latter as a mid-range estimate for Sr from Figure 8.11 in Fairchild and Baker (2012):

$[Mg]_{PCP} = [Ca]_{PCP} \times [Mg/Ca]_{PCP}$, since $K_{Mg}=[Mg/Ca]_{solid}/[Mg/Ca]_{aqueous}$, this becomes

$$[Mg]_{PCP} = [Ca]_{PCP} \times [Mg/Ca]_{dripwater} \times K_{Mg}, \quad [4]$$

Bedrock contribution is estimated by: $[Mg]_{bedrock} = [Ca]_{initial} \times [Mg/Ca]_{bedrock}$ [5]

The residual component is calculated by:

$$[Mg]_{residual} = [Mg]_{dripwater} - [Mg]_{marine\ aerosol} - [Mg]_{bedrock} + [Mg]_{PCP} \quad [6]$$

The use of Cl ratios in equation 1 effectively corrects for the effect of ion exclusion by transpiration. In quantifying aerosol and bedrock contributions, it is assumed that the potential uptake of Cl and Ca by biomass is small. For Cl, this is supported by dendrochemical studies on these *E. diversicolor/C. calophylla* forests: for example, Grove and Malajczuk (1985; Table 8) measured a Cl uptake rate of 11-47 kg/ha/a, equivalent to 2-8 mg/l or <10% in our dripwaters (assuming mean P-AET of 600 mm/a). Calcium sequestration rates of 30-60 kg/ha/yr (Grove and Malajczuk, 1985) could have a potential impact on our dripwaters (equivalent to 5-10 mg/l or 7-20%). This may result in an underestimate of the amount of carbonate dissolution hence bedrock-derived ions in our mass balance. For both Cl and Ca, fluxes to and from the biomass are balanced in mature forests (Grove and Malajczuk, 1985). However, in the current study the system may not be in balance due to the regeneration from the fire in 2006 and some minor loss of Ca and Cl due to biomass accumulation may be expected.

5.3 Mass balance data

The relative contributions from marine aerosol, bedrock and residuals, calculated via our mass balance are summarised in Table 5. As expected, Sr is dominated at all sites by input from bedrock weathering. In the first instance we adopted the bedrock Sr/Ca ratio given by the bulk composition for each chamber reported in Table 1. For sites 1A and 1B, this resulted in residual values of zero i.e. bedrock contributions were close to 100%. For sites 2A, 2B and 2E, this resulted in a relatively higher positive Sr residual value (0.06 mg/l). This higher than expected positive residual for a bedrock-derived element could be a consequence of our assumption of no net Ca uptake by biomass (Section 5.2), or that the bulk composition determined for chamber 2 may not be representative. Applying the Sr/Ca ratio from chamber 1 to chamber 2, reduced the residual and brought the bedrock contribution closer to 100% as reported in Table 5. Apart from Ca, which is excluded by definition as discussed in Section 5.2, no other ions are dominated by bedrock input (Table 5), although Si was not included in the mass balance as neither our experimental determination of bedrock bulk Si/Ca nor the value used for seawater Si/Cl might be representative of field conditions (Section 4.1).

Table 5: Contribution of aerosol and bedrock end-members to dripwater ions calculated via mass balance. The residual term indicates an additional source (positive values) or a sink (negative values).

	1A mg/l	1B mg/l	2A mg/l	2B mg/l	2E mg/l
Sr					
Aerosol	0.05	0.05	0.04	0.07	0.06
Bedrock	0.16	0.16	0.17	0.18	0.21
Residual	0.01	0	-0.03	-0.04	-0.08
Na					
Aerosol	67.6	69.4	57.1	90.1	82.1
Bedrock	0	0.00	0.00	0.00	0.00
Residual	-3.8	-2.9	-3.6	-10.6	-5.4
K					
Aerosol	2.5	2.5	2.1	3.3	3.0
Bedrock	0.05	0.05	0.02	0.02	0.02
Residual	-1.6	-1.6	-0.56	-1.7	-1.5
Mg					
Aerosol	8.0	8.2	6.8	10.7	9.71
Bedrock	0.37	0.37	0.33	0.35	0.47
Residual	-1.1	-1.2	0.68	-2.9	-2.5
SO_4					
Aerosol	16.8	17.3	14.2	22.4	20.4
Bedrock	0.10	0.10	0.01	0.01	0.01
Residual	-9.0	-9.3	-2.1	-13.1	-12.2

Dripwater Na, K, Mg and SO_4 concentrations are dominated by aerosol contribution (Table 5; 62% or greater) which is consistent with the high aerosol flux at this site (Hingston and Gailitis, 1976). However, these ions have negative residuals for most sites indicating significant sink(s) along the

flow path. Sulphate has the largest sink: 12-13 mg/l representing 53-60% of dripwater SO_4 for sites 2B and 2E, but less (15%) for site 2A (Table 5). The magnitude of the sinks for Mg (9-27%) and K (27-61%) are also significant, and similarly impact site 2A least and site 2B the most (Table 5). The sink for Na is minor (<11% of dripwater Na).

Magnesium, SO_4 and K ions constitute macro-nutrients for vegetation (Mengel et al., 2001). It is likely that large quantities of these aerosol-sourced ions are taken up as nutrients by forest growth as observed from shallow groundwaters elsewhere (Dean et al., 2014). A significant level of nutrient-uptake is consistent with the high impact of transpiration on these dripwaters and confirms the important role of vegetation processes in modifying dripwater concentrations. In fact, the magnitude of the residuals for K, Mg and SO_4 (indicating nutrient uptake) increase in the same order as the Cl concentrations (indicating transpiration) across the sites (Section 4.2). Moreover, this spatially-based relationship further confirms that site 2A is the least impacted by vegetation processes, whilst site 2B is the most affected.

An alternative sink for sulphate requiring consideration is reduction to sulphides. However, isotope ($\delta^{34}S$-SO_4 and $\delta^{18}O$-SO_4) investigations on these dripwaters do not support this mechanism (Section 4.3). If sulphate reduction were a dominant process, dripwater $\delta^{18}O$-SO_4 would have been expected to be isotopically-enriched relative to rainwater (Wynn et al., 2008; Wynn et al., 2013). Rather, a 2‰ depletion was observed, consistent with a biomass sink.

The time series of residuals (Fig. 6) shows a distinct trend towards more strongly negative residuals for SO_4, suggesting that biomass assimilation of sulphur is increasing through time (Fig. 6), although less so for site 2A. Disregarding site 2A, this nutrient uptake is greatest in magnitude and through time in chamber 2 versus chamber 1. The magnitude of the overall decrease in residuals for SO_4 is about 4 mg/l (site 2B): more than twice the overall change measured in dripwater SO_4 concentrations (Fig. 3) suggesting that water extraction by transpiration (which increases solute

concentrations in the remaining pore water) is masking the full signal of sulphur assimilation into the biomass.

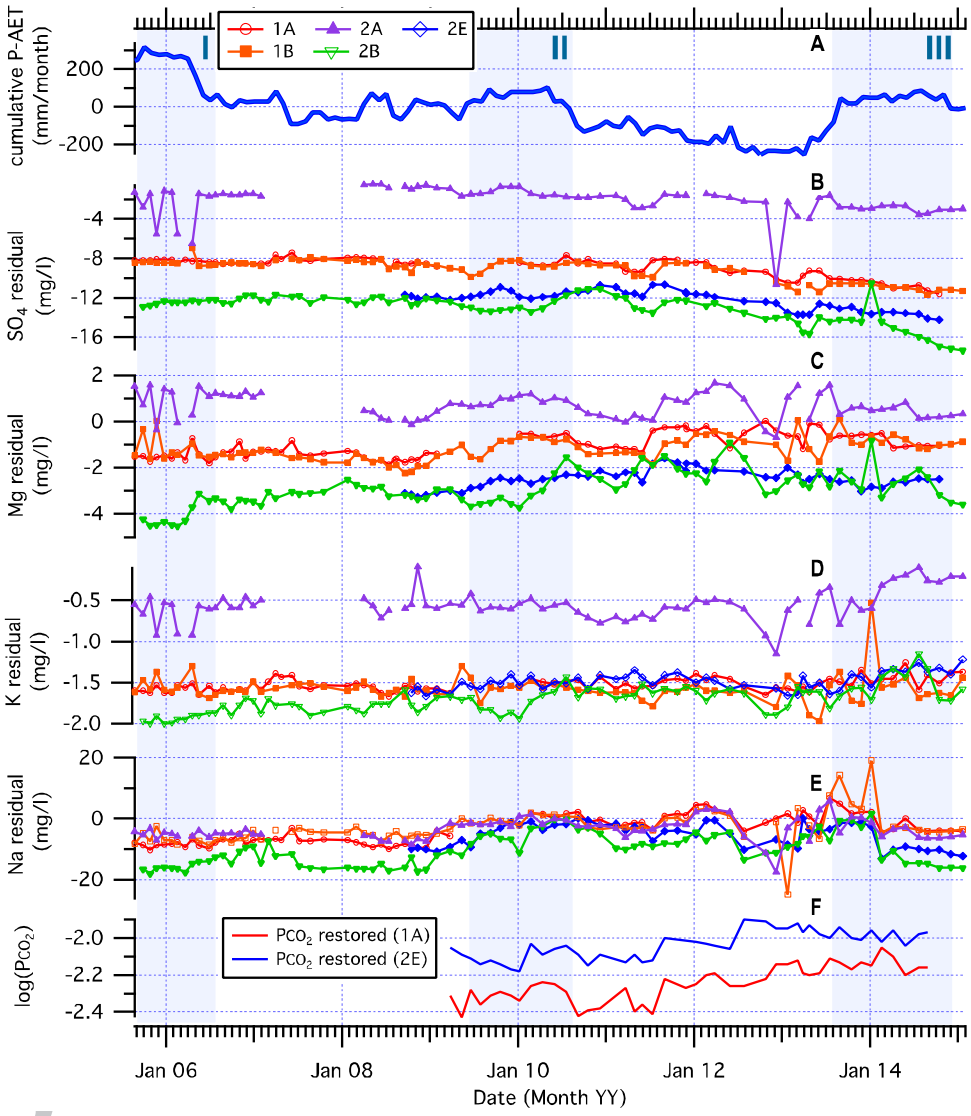

Figure 6: Time series of cumulative P-AET (A), calculated residuals for SO_4, Mg, K,and Na for dripwater (B-E) as well as restored P_{CO_2} from Treble et al. (2015) (F). More negative residuals indicate greater sink. Restored P_{CO_2} is the reverse modelled CO_2 that the solution originally equilibrated with and represents CO_2 source production in the unsaturated zone. These data from Treble et al. (2015) are updated to August 2014 here. The three vertical blue bars, labelled I-III, indicate periods of higher cumulative P-AET coinciding with increased drip rates at some sites indicating enhanced recharge.

Magnesium residuals at sites 2B and 2E closely follow an overall rising trend until this reverses and declines from ~2012 onwards, following an approximate inverse trend with cumulative P-AET. Similar behaviour is evident for sites 1A and 1B, but the trends are less pronounced, consistent with the biomass sink being overall less effective at these two sites. The stronger biomass connection at site 2B, is also evident in the seasonal signals, appearing from 2010 onwards. Magnesium residuals peak in winter months, becoming more negative through spring indicating an increasing sink that is consistent with increasing biomass uptake through the spring growth season (Figure 6). There appears to be no overall trend in the K residuals, although there is a shift in mean values at site 2B during 2010 (from a more to a less effective sink), with occasional seasonal cycles also appearing after this shift coinciding with those noted in the Mg residuals for this site (Fig. 6).

The Na residuals are persistently negative for the first three years of our study but move closer to zero during the second recharge period (Figure 6). They become more strongly negative when cumulative P-AET is lowest, prior to the third recharge interval when residuals again return to zero or become positive, before becoming negative again during 2014. The relationship between cumulative P-AET and Na-residuals suggests that the effectiveness of the Na sink is hydrologically-related, and is consistent with a higher Na flux to the 'soil store' (Figure 5) in drier years. However, our soil leaches showed that the contribution of NaCl from soil salts is very small and this is supported by our mass balance calculations as well as the lack of evidence for evaporation in our dripwaters (Treble et al., 2013). Likely processes determining the sink for Na are clay mineral reactions either in the form of reverse ion exchange or clay mineral formation in the soil zone: Table 2 shows that dripwater Cl is in excess relative to Na which supports this process. Additionally, the delay by several months of the maxima in Na versus Cl during 2009-2010 in our time series for site 2B suggests that the cation exchange capacity in the unsaturated zone is slowing the transport of Na, relative to Cl. Further investigation on the cation exchange capacity and clay mineralogy of these soil and rock samples would be needed to define this process.

5.4 Water and nutrient uptake by biomass

We interpret from our PCA that dripwater ion concentrations in this study are dominated by transpiration and that the impact of transpiration is increasing through time. The calculated residuals in our mass balance suggest that nutrient uptake is similarly increasing through the duration of the study. These trends are consistent with rising PCO_2 in the vadose-zone calculated from this dataset by Treble et al. (2015) (Fig. 6). Thus the evidence consistently points to the increasing impact of the forest biomass on these dripwaters over the duration of the study. Furthermore, the vegetation signals (transpiration, assimilation plus PCO_2) in the dripwater are strongest in chamber 2 sites 2B and 2E, demonstrating spatial variability with sites 2B and 2E apparently have a stronger association with vegetation above the cave.

The nutrient uptake signal dominates dripwater SO_4 concentrations which is consistent with the high nutrient demand for S in these forests (third highest requirement, after N and P; O'Connell and Grove, 1996). The understorey in SW Australian *E diversicolor* forests in particular contains about half of the S in the total above-ground biomass (O'Connell and Grove, 1996 and references therein). Sulphur is preferentially stored in biomass foliage (Grove and Malajczuk, 1985; O'Connell and Grove, 1996) and S is the most volatile of these ions considered in this study. Large amounts of S may be exported from the local catchment by fire (O'Connell and Grove, 1996) or redistributed in ash fall (Yusiharni and Gilkes, 2012). Hence the S budget will be particularly sensitive to understory disturbance and regrowth.

The strong negative trend in SO_4 residuals (increasing assimilation) is thus consistent with observations of a thickening understory over the duration of this study aided by enhanced regrowth following the fires in early 2006 (Section 2.3). As fire results in the redistribution of nutrients including sulphur from the biomass to soil, via ash (Grove et al., 1986) a further possible explanation for the prominence of the downward trend in our dripwater SO_4 concentrations, is that the fire

released S at the beginning of our monitoring, and this S has become increasingly depleted (e.g. source-limited) over time as the understorey recovers (e.g. Dean et al., 2014).

A second hypothesis for the increasing impact of vegetation processes on these dripwater data is the maturing of the marri and karri eucalypt trees overlying Golgotha Cave. The observation that tree-roots emerge from the cave ceiling (Section 2.3), suggests that transpiration could be occurring throughout the vadose zone above Golgotha Cave. The variable distance between dripwater sampling sites and the root system may explain the spatial variability in dripwater solutes due to both transpiration and nutrient uptake. Tree age may contribute to this spatial variability, as well as temporal variability, since although net transpiration and assimilation slow with forest maturity overall, the demand by individual trees continues to rise whilst they are growing (MacFarlane et al., 2010; Grove and Malajczuk, 1985).

5.5 Are long-term trends driven by vegetation growth or a drying climate?

The interpretation of the long-term rising trend in these solute data suggests that transpiration has risen through the monitoring period. To examine a third hypothesis: that a long-term rise in transpiration may be climate-driven; AWAP modelled AET, soil evaporation, transpiration, precipitation and temperature (Raupach et al., 2009) are shown in Figure 7. These data support our inference that AET is largely a function of transpiration rather than soil water evaporation at this location (Fig. 7). Temperature has risen by approximately 1°C over the duration of monitoring; evident in mean, minimum and maximum temperature anomalies at the cave site, particularly from 2010 onwards (Fig. 7) and is consistent with observations from surrounding stations (Bureau of Meteorology, 2015). Despite the warming, modelled AET is either unchanged (with respect to the trend in mean AET) or declining (with respect to the trend in max AET) through the monitoring study (Fig. 7). Thus AWAP modelled data suggest that there has been *no overall rise in transpiration in response to climate* over the duration of the monitoring study. The modelled data further suggest that transpiration in this system is water-, rather than energy-limited.

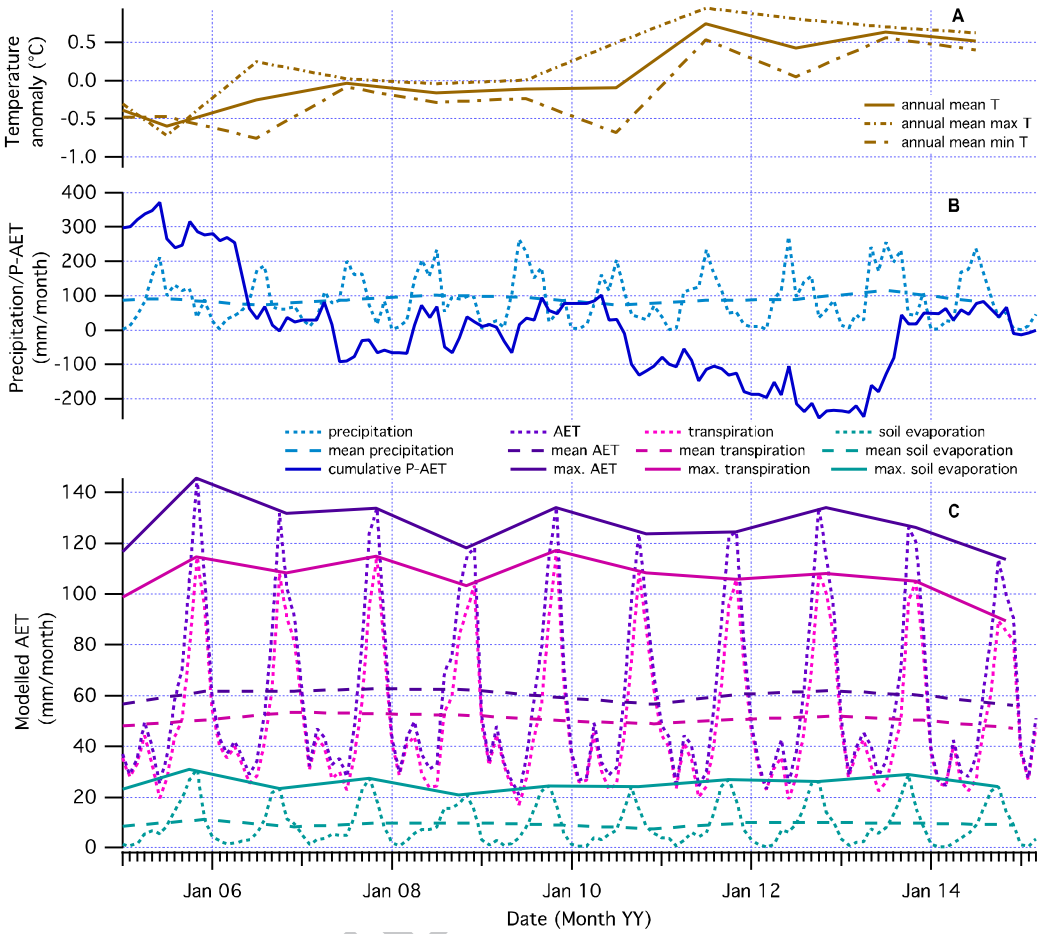

Figure 7: Temperature anomalies (A), precipitation and cumulative sum of P-AET (B) and estimated soil evaporation, transpiration and total AET (C) at Golgotha Cave during the cave monitoring study. Estimated AET, transpiration and soil evaporation are parameters FWE, FWTra and FWsoil, respectively, from AWAP (Raupach et al., 2009).

The above comparison supports the conclusion that the inferred rise in transpiration in the dripwater dataset, may be predominantly attributed to vegetation processes: either post-fire recovery of the understorey and/or tree maturity. Evidence of vegetation processes are supported by the coincident rise in modelled vadose-zone P_{CO_2}, which was attributed to an increase in biomass and root respiration following fire (Treble et al., 2015), and is also supported by the increasing uptake of SO_4 by vegetation in this study. Considering this, total transpiration is likely to have increased by up to 20% over this time, based on Cl concentrations. A significant proportion of this increase is likely to be additional transpiration from understorey regrowth or tree maturation, but

quantification of these contributions is beyond the scope of this study. This reflects two areas of uncertainty with respect to the behaviour of the system following a fire:

First, over the period of the monitoring study there will be changes in the partitioning of total evapotranspiration between evaporation (from the soil), understorey transpiration and overstorey transpiration. Changes in soil structure, and in the proportion of bare ground, post-fire will affect actual evaporation rates. Transpiration from understorey vegetation is likely to have fallen substantially immediately after the fire, albeit recovering quickly, but the effects of fire on overstorey transpiration are unknown. Hence the estimated transpiration rates should be interpreted with caution.

Second, changes in the water balance can be anticipated immediately post-fire. These could reflect changes in soil structure, principally in organic matter content and the forest litter, which would affect the soil's ability to retain moisture, thereby increasing the proportion of precipitation that percolates at depth into the limestone. The modelled AET rates plotted may therefore be an overestimate, although the time required for the shallow water flow pathways to revert to their state prior to the fire, is unknown.

In the case of the 2006 fire, the impact on the forest was spatially variable with the main impact being patchy removal of the understorey (according to field observations approximately one month post-fire). There has since been a general thickening of the understorey throughout the duration of monitoring study, which is not limited to the actual burnt patches, suggesting that the regrowth may be more related to recovery from the hotter wildfire in 1992 that had a more extensive impact on vegetation directly above and within the cave catchment (Section 2.3).

In reality, it is difficult to isolate climate versus vegetation growth impacts, particularly as forest recovery will be influenced by the water balance and growth will be further limited during periods of water stress. For example, recharge interval III may have assisted in stimulating growth, enhancing

transpiration and facilitating forest recovery. It should also be noted that this study began five years into a strong downward trend in cumulative P-AET occurring since 2000 CE, driven by below average rainfall. This downward trend in the water balance (evident in the cumulative P-AET curve; Fig. 7) is further embedded in a recognised longer-term interval of climate change that has resulted in progressive drying of the SW Australian region since around 1970 CE (Bates et al., 2008). Hence, it cannot be ruled-out that the 10-year trend in this study is not partially driven by the longer-term impact of the drying climate on the forest ecosystem.

5.6 Biomass influence on spatial variability in dripwater solute concentrations and flow paths

Biomass has a significant impact on modulating the dripwater solute concentrations at the studied site. The greatest impact is at sites 2B and 2E, and the least at site 2A. The distinct spatial variability in biomass impact may be explained by the proximity of flow paths in the bedrock to tree roots as depicted in Figure 8.

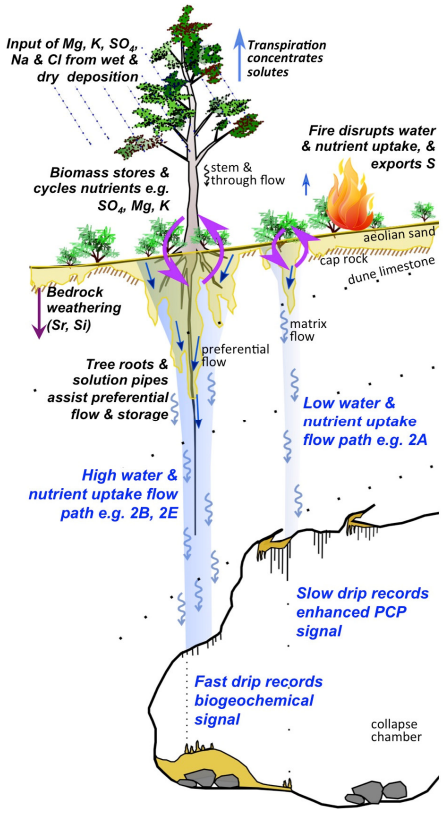

Figure 8: Conceptual model illustrating key processes acting on Golgotha Cave system based on this study and Treble et al. (2015). Forest biomass impacts on dripwater chemistry via the concentration of solutes by transpiration and by nutrient uptake. Flow paths are influenced by deeply-rooted trees creating preferential flow paths and potential water storage. The two contrasting flow paths illustrate the greater influence of biomass on sites 2B and 2E versus site 2A.

This spatial variability in dripwater concentrations confirms distinct hydrological pathways feeding Golgotha Cave dripwaters (Treble et al., 2015) as well as providing supporting evidence for tree roots to promote flow paths, permitting preferential water movement to greater depths along root channels (Jennings, 1968; Peck et al., 1981; Fig. 8), as well as the potential for water storage along these flow paths. The timing of the arrival of the seasonal signal in dripwater concentrations at site 2B, consistent with enhanced growth during spring, suggests that there is minimal lag that might be expected due to transit time, further supporting preferential flow-paths. Given the strong evidence for matrix-flow at these sites (Section 2.2) this influence probably decreases with depth, as drip rates appear to be ultimately determined by matrix permeability above the ceiling (Mahmud et al., 2015a; 2015b).

5.7 Implications for speleothem trace element records

This study has demonstrated the potential for S to be used to track biomass changes in the Golgotha Cave speleothem record via its importance as a nutrient in these forests. In fire-prone regions such as SW Australia, speleothem S could serve as a particularly useful proxy to reconstruct past fire history. Speleothem S may be measured quantitatively via SIMS (e.g. Wynn et al., 2010). The approximate decline in dripwater SO_4 concentrations over the study period is 1.4 mg/l, calculated using the averages of the first and final six months of monitoring. Applying the partition coefficient for S/Ca from dripwater to speleothem used by Borsato et al. (2015), yielded an estimated decline in

speleothem calcite equivalent to 47 ppm, well above the analytical precision of several ppm for SIMS (e.g. Wynn et al., 2010).

With regards to the other ions studied, Mg, K, Na and Cl could potentially be useful for tracking transpiration in dripwater. But whether this transpiration signal translates to the speleothem will depend on whether transpiration alters the dripwater ion/Ca ratio. For example, if transpiration concentrates both ions similarly, there would be no change in this ratio in the dripwater, hence nor in the resulting concentration of this ion in the speleothem. Alternatively, if transpiration resulted in the enhanced uptake of Ca relatively to these other ions by biomass, this would raise the concentration of these ions in the speleothem. Uptake of Ca as a plant nutrient exceeds Mg, Na and Cl, by two times or greater, based on measurements in leaf and stem tissue (Grove and Malajczuk, 1985; O'Connell and Grove, 1996), but transpiration and nutrient assimilation are largely independent processes (Sands and Mulligan, 1990). For example, peak water and nutrient uptake will vary seasonally according to water availability (Sands and Mulligan, 1990) and this is supported by the difference in seasonal maxima in PC1 (Section 5.1) and Mg residuals (Section 5.3). Further to this, it is difficult to assess this process in our data. For example, maximum Mg/Ca values (coinciding with Golgotha Cave's non-ventilated mode when PCP is minimal) at sites 1A and 1B, show no overall change over the study duration as the rise in Mg is counteracted by the rise in Ca (Fig. 3); the latter was attributed to increased bioproductivity (Treble et al., 2015).

During periods of lower rainfall, waters in the vadose zone have a longer mean residence time providing greater opportunities for water-rock interaction and leading to a rise in dripwater Sr concentrations. It seems that this increase is independent of biomass activity other than the transpiration. Thus, trends in Sr are potentially useful proxies of the vadose zone residence time and hence a measure of the recharge variability in speleothems.

It should be highlighted that only dripwater has been considered here and that Treble et al. (2015) demonstrated that in-cave PCP may ultimately dominate the stalagmite trace element data from the

low-flow sites, as depicted in Fig. 8. Thus speleothem trace element records that potentially inform on variations in aerosol flux, bedrock dissolution, forest bioproductivity etc, may be limited to stalagmites fed by high-flow drips in Golgotha Cave. This includes speleothem Mg and Sr as it is known that these ions are sensitive to PCP. Finally, some elements in this study do not behave predictably in terms of their incorporation from dripwater into speleothems: this is the case for Na and Cl (Huang & Fairchild, 2001; Fairchild & Baker, 2012) and typical speleothem K concentrations are also not known.

6 CONCLUSIONS

At this coastal site, the source of many of the ions in dripwaters are from aerosols but it is concluded that transpiration and nutrient uptake by forest biomass significantly modify this signal resulting in spatial and temporal variability in solute concentrations entering the cave. These findings suggest that deeply-rooted trees are interacting with the shallow vadose-zone hydrochemistry causing the variable dripwater chemistry in Golgotha Cave. This is the first time that the impact of biomass on major and minor concentrations in dripwater has been quantitatively explored. We suggest that the implications of these findings are highly relevant to any karst system in a forested catchment or anywhere that transpiration has a significant role in the water balance.

Of the five monitored sites, site 2A was least impacted by vegetation processes while sites 2B and 2E were most strongly impacted. All sites display smooth long-term trends, interpreted as a disruption to a previous steady-state by a fire and subsequent forest regeneration and/or maturing of the overlying trees. Both scenarios are consistent with the evidence for rising CO_2 in the unsaturated zone, from Treble et al. (2015). As it is anticipated that the impacts of either scenario are similar, we cannot further distinguish the dominant process in this study. It also cannot be ruled-out that this response is also superimposed on longer-term climate-driven changes in hydrology. Hence, continuation of the Golgotha Cave monitoring study as well as additional instrumentation such as sap-flow meters, is warranted to better understand the longer-term climate driven impacts and tree

maturity versus shorter-term disruptions to the system such as fire. Dripwater Sr and Si may be a more straight-forward indicator of recharge variation, via their release by weathering, and their lessor roles as biomass nutrients.

An interesting outcome of this study is the possibility that a signal of biomass recovery after fire may be present in speleothem records. Speleothem S may be a particularly sensitive fire-proxy, particularly if fire causes it to be source-limited, extending the persistence of this signal in the dripwater. While this may be a relatively short-term signal, it is potentially detectable as the impact of forest regeneration may generate hydrochemical signals persisting for up to fifteen years (O'Connell and Grove, 1996; Coleborn et al., in press). We propose to further investigate the impact of fire on our speleothem records in a future study by re-examining our high-resolution trace elements from modern speleothems (e.g. Treble et al., 2003) against the known fire history for their catchments. A more complete characterisation of S including isotopes in this system is also warranted.

Acknowledgements

We gratefully acknowledge and thank the following people for their assistance with fieldwork and sample analyses: Monika Markowska, the staff of Calgardup Cave, Henri Wong, Andy Spate, Mark Tozer, Paul Rustomji, Carol Tadros and Kashif Mahmud. We also thank the WA Department of Parks and Wildlife for fire history information, Anne Ankcorn for cartography, and Sebastian Breitenbach and two anonymous reviewers for thoughtful reviews that improved the final manuscript. The Golgotha Cave map was reproduced in modified form with permission from Barry Loveday's 1997 survey. This study was initiated with funding from Land & Water Australia (ANU52) grant to PT. Some ideas were generated from ARC Linkage Project LP130100177 awarded to AB, IJF and PCT and

the outcomes of this study contribute to ARC Discovery Project DP140102059 awarded to PCT. This is paper number 11 of the Birmingham Institute for Forest Research.

List of table captions

Table 1: Summary of leachate concentration data for crushed bedrock and soil samples, as well as bulk composition determined by acid digestion. Units are mg per kg of solid. Anion data were only obtained for leachates hence elemental S values are reported for bulk composition rather than SO_4. Values for cave chamber 1 bulk and chamber 2 bulk (bold italics) are used to estimate bedrock contribution in mass balance calculations (Section 5.2, equation 5).

Table 2: Summary of dripwater and rainwater chemistry between August 2005 and January 2015. Drip rate (Treble et al., 2013) is converted to discharge assuming a drip volume of 0.2 ml (Collister and Mattey, 2008).

Table 3: List of samples analysed for sulphate isotopes. Dash indicates insufficient sample for analysis.

Table 4. Results of PCA on the entire dataset (n = 308): numbers indicate positive or negative loading (analogous to a correlation coefficient) of each parameter on each principal component. The bottom row gives the total percentage of variation in the data explained by each component.

Table 5: Contribution of aerosol and bedrock end-members to dripwater ions calculated via mass balance. The residual term indicates an additional source (positive values) or a sink (negative values).

List of figure captions

Figure 1A-C: Longitudinal cross section view of Golgotha Cave showing sampling areas (A); the location of Golgotha Cave, southwest Western Australia (B); and photograph of mixed karri-marri forest above Golgotha Cave (C). See Figure 1 in Treble et al. (2015) for plan view of cave. The brown square indicates the location of the soil sampling pit and green triangles indicate the location of bedrock samples collected for this study (see Table 1 for further information).

Figure 2A-C: Differential normalised burn ratio (dNBR) image created using Landsat 5 TM data pre-fire (28/2/2006) and post-fire (12/5/2006) (A); pre-fire (4/11/1992) and post-fire (6/12/1992) (B); and average dNBR index per pixel calculated for the larger catchment area for the cave, the area directly above the cave, an unburned background patch and the wider regional fire extent limited to Boranup Karri Forest (see Fig. 1B) for fires in 1992, 1998 and 2006 (C). Location of Golgotha Cave entrance is indicated by yellow dot and black line is the main passageway; white dashed line is the catchment area for Golgotha Cave. The catchment area was calculated by GIS analysis of digital elevation model data (Farr et al., 2007; Gallant et al., 2011). Insets shows the full extent of the larger 1800 Ha 2006 fire, indicated by brown colour, using the post-fire Landsat 5 TM imagery with Bands 3-2-1.

Figure 3: Time series of P-AET (shaded), cumulative P-AET (blue line) (A), drip rate (B), Cl, Na, K, Mg, Si, Sr, SO_4 and Ca data (C-J) at each of the drip sites for Golgotha Cave. Monthly P-AET is calculated using precipitation minus modelled actual evapotranspiration (parameter 'FWE') extracted at our location from the AWAP database (Raupach et al., 2009; 2011). Cumulative P-AET or "residual mass curve" following Hurst (1951) is calculated as the cumulative sum of the monthly P-AET anomaly. The three vertical blue bars, labelled I-III, indicate periods of higher cumulative P-AET coinciding with increased drip rates at some sites indicating enhanced recharge.

Figure 4: Time series of P-AET (shaded), cumulative P-AET (blue line) (A) and the scores of the principal components: PC1 (B), PC2 (C) and PC3 (D); of dripwater Ca, Mg, Na, K, Si, Cl, SO_4 and PCO_2. The three vertical

blue bars, labelled I-III, indicate periods of higher cumulative P-AET coinciding with increased drip rates at some sites indicating enhanced recharge.

Figure 5. Box model to illustrate mass balance approach to modelling Golgotha dripwater hydrochemistry. Blue arrows indicate water flux and black arrows indicate elemental fluxes. The mass balance used is summarised at the bottom of the diagram; pollution and dust dissolution flux is minor and subsumed under bedrock dissolution.

Figure 6: Time series of cumulative P-AET (A), calculated residuals for SO_4, Mg, K,and Na for dripwater (B-E) as well as restored Pco_2 from Treble et al. (2015) (F). More negative residuals indicate greater sink. Restored Pco_2 is the reverse modelled CO_2 that the solution originally equilibrated with and represents CO_2 source production in the unsaturated zone. These data from Treble et al. (2015) are updated to August 2014 here. The three vertical blue bars, labelled I-III, indicate periods of higher cumulative P-AET coinciding with increased drip rates at some sites indicating enhanced recharge.

Figure 7: Temperature anomalies (A), precipitation and the cumulative sum of P-AET (B) and estimated soil evaporation, transpiration and total AET (C) at Golgotha Cave during the cave monitoring study. Estimated AET, transpiration and soil evaporation are parameters FWE, FWTra and FWsoil, respectively, from AWAP (Raupach et al., 2009).

Figure 8: Conceptual model illustrating key processes acting on Golgotha Cave system based on this study and Treble et al. (2015). Forest biomass impacts on dripwater chemistry via the concentration of solutes by transpiration and by nutrient uptake. Flow paths are influenced by deeply-rooted trees creating preferential flow paths and potential water storage. The two contrasting flow paths illustrate the greater influence of biomass on sites 2B and 2E versus site 2A.

References

Appelo, C.A.J, and Postma, D., 2007. Geochemistry, groundwater and pollution. A.A. Balkema Publishers, London (2nd edition), 649pp.

Baker, A., Brunsdon, C., 2003. Non-linearities in drip water hydrology: an example from Stump Cross Caverns, Yorkshire. *Journal of Hydrology* 277, 151-163.

Baker, A., Genty, D., Fairchild, I.J., 2000. Hydrological characterisation of stalagmite drip waters at grotte de Villars, Dordogne, by the analysis of inorganic species and luminescent organic matter. *Hydrology and Earth System Science* 4, 439-450.

Baker, A., Smith, C.L., Jex, C., Fairchild, I.J., Genty, D. and Fuller, L., 2008. Annually laminated speleothems: a review. *International Journal of Speleology* 37, 193-206.

Baldini, J.U.L., McDermott, F., Baker, A., Baldini, L.M., Mattey, D.P., Railsback, L.B., 2005. Biomass effects on stalagmite growth and isotope ratios: A 20th century analogue from Wiltshire, England. *Earth and Planetary Science Letters* 240, 486-494.

Baldini, J.U.L., McDermott, F., Fairchild, I.J., 2006. Spatial variability in cave drip water hydrochemistry: Implications for stalagmite paleoclimate records. *Chemical Geology* 235, 390-404.

Bates, B.C., Hope, P., Ryan, B., Smith, I. & Charles, S., 2008. Key findings from the Indian Ocean Climate Initiative and their impact on policy development in Australia. *Climatic Change* 89, 339-54.

Borsato, A., Frisia, S., Fairchild, I.J., Somogyi, A., Susini, J., 2007. Trace element distribution in annual stalagmite laminae mapped by micrometer-resolution X-ray fluorescence: Implications for incorporation of environmentally significant species. *Geochimica et Cosmochimica Acta* 71, 1494-1512.

Borsato, A., Frisia, S., Wynn, P., Fairchild, I.J. & Miorandi, R., 2015. Sulphate concentration in cave dripwater and speleothems: long-term trends and overview of its significance as proxy of environmental processes and climate forcing. *Quaternary Science Reviews (*in press).

Bureau of Meteorology, 2014. Climate statistics. http://www.bom.gov.au/climate/data/ (accessed 15.01.14).

Bureau of Meteorology, 2015. Climate statistics. http://www.bom.gov.au/climate/change/ (accessed 18/11/15).

Calhoun, J.A., Bates, T.S., Charlson, R.J., 1991. Sulfur isotope measurements of submicrometer sulphate aerosol-particles over the Pacific Ocean. *Geophysical Research Letters* 18, 1877-1880.

Chester, R.1990 Marine Geochemistry, Unwin Hyman, Boston

Coleborn, K., Spate, A., Tozer, M., Andersen, M.S., Fairchild, I., MacKenzie, B., Treble, P., Meehan, S., Baker, A. & Baker, A. (in press): Effects of wildfire on long-term soil CO_2 concentration: Implications for karst processes. *Environmental Earth Sciences*.

Collister, C., Mattey, D., 2008. Controls on water drop volume at speleothem drip sites: An experimental study. *Journal of Hydrology* 358, 259-267.

Cruz, F.W., Burns, S.J., Jercinovic, M., Karmann, I., Sharp, W.D., Vuille, M., 2007. Evidence of rainfall variations in Southern Brazil from trace element ratios (Mg/Ca and Sr/Ca) in a Late Pleistocene stalagmite. *Geochimica Et Cosmochimica Acta* 71, 2250-2263.

Cuthbert, M.O, Baker, A., Jex, C.N., Graham, P.W., Treble, P.C., Andersen, M.S., Acworth, R.I., 2014. Drip water isotopes in semi-arid karst: implications for speleothem paleoclimatology. *Earth and Planetary Science Letters* 395, 194-204.

DPaW (Department of Parks and Wildlife WA), 2012. Fire history map: Calgardup Cave to Golgotha Cave, Kirup Fire Management Services, generated 23/10/2012.

Fairchild, I.J. & Hartland, A. 2010 Trace element variations in stalagmites: controls by climate and by karst system processes. In: Stoll, H. and Prieto, M., editors. *Ion partitioning in ambient temperature aqueous systems: from fundamentals to applications in climate proxies and environmental geochemistry*. EMU Notes in Mineralogy, 10, 259-287.

Fairchild, I.J., Baker, A., 2012. *Speleothem Science: From Process to Past Environments.* Wiley-Blackwell, Oxford.

Fairchild, I.J. & Frisia, S. 2014 Definition of the Anthropocene: a view from the underworld. In: Waters, C., Zalaciewicz, J., Williams, M., Ellis, M.A. & Snelling A. et al. (eds.) *A Stratigraphical Basis for the Anthropocene.* Geological Society Special Publication 395, 239-254.

Fairchild, I.J., Borsato, A., Tooth, A.F., Frisia, S., Hawkesworth, C.J., Huang, Y., McDermott, F., Spiro, B., 2000. Controls on trace element (Sr-Mg) compositions of carbonate cave waters: implications for speleothem climatic records. *Chemical Geology* 166, 255-269.

Fairchild, I.J., Loader, N.J., Wynn, P.M., Frisia, S., Thomas, P.A., Lageard, J.G.A., de Momi, A., Hartland, A., Borsato, A., La Porta, N. and Susini, J. 2009 Sulfur fixation in wood mapped by synchrotron X-ray studies: implications for environmental archives. *Environmental Science and Technology,* 43, 1310–1315.

Fairchild, I.J., Spötl, C., Frisia, S., Borsato, A., Susini, J., Wynn, P.M., Cauzid, J. & EIMF, 2010. Petrology and geochemistry of annually laminated stalagmites from an Alpine cave (Obir, Austria): seasonal cave physiology. In: Pedley, H.M.& Rogerson, M. (eds) Tufas and Speleothems: Unravelling the Microbial and Physical Controls. *Geological Society, London, Special Publication*, 336, 295–321.

Farquhar, G.D., Cernusak, L.A. & Barnes, B., 2007. Heavy water fractionation during transpiration. Plant Physiology, 143: 11-18. doi: 10.1104/pp.106.093278

Farr, T.G., Rosen, P.A., Caro, E., Crippen, R., & et al., 2007. The shuttle radar topography mission. *Reviews of Geophysics*, 45, RG2004.

Frisia, S., Borsato, A., Fairchild, I.J., Susini, J., 2005. Variations in atmospheric sulphate recorded in stalagmites by synchrotron micro-XRF and XANES analyses. *Earth and Planetary Science Letters* 235, 729-740.

Gallant, J.C., Dowling, T.I., Read, A.M., Wilson, N., Tickle, P., Inskeep, C. (2011) 1 second SRTM Derived Digital Elevation Models User Guide. Geoscience Australia

Grove, T.S. and Malajczuk, N., 1985. Nutrient accumulation by trees and understorey shrubs in an age-series of *Eucalyptus diversicolor F. Muell*. stands. *Forest Ecol Manag* 11, 75-95.

Hall, G.J., Marnham, J.R., 2002. Regolith-landform Resources of the Karridale-Tooker and Leeuwin 1:50000 sheets. Dept. of Mineral and Petroleum Resources, Geologogical Survey of Western Australia, Perth 74 pp.

Hansen, M., Dreybrodt, W., Scholz, D., 2013. Chemical evolution of dissolved inorganic carbon species flowing in thin water films and its implications for (rapid) degassing of CO_2 during speleothem growth. *Geochimica et Cosmochimica Acta* 107, 242-251.

Hartland, A., Fairchild, I.J., Lead, J.R., Borsato, A., Baker, A., Frisia, S., Baalousha, M., 2012. From soil to cave: Transport of trace metals by natural organic matter in karst dripwaters. *Chemical Geology* 304, 68-82.

Hingston, F.J. and Gailitis, V., 1976. The Geographic variation of salt precipitated over Western Australia. *Australian Journal of Soil Research* 14, 319-335.

Hori, M., Ishikawa, T., Nagaishi, K., You, C.F., Huang, K.F., Shen, C.C. and Kano, A., 2014. Rare earth elements in a stalagmite from southwestern Japan: A potential proxy for chemical weathering. *Geochem J* 48, 73-84.

Huang, Y., Fairchild, I.J., 2001. Partitioning of Sr2+ and Mg2+ into calcite under karst-analogue experimental conditions. *Geochimica et Cosmochimica Acta* 65, 47-62.

Hurst, H., 1951, Methods of long-term storage in reservoirs: Transactions of the American Society of Civil Engineers, vol. 116, p. 519 – 543.

Johnson, K.R., Ingram, B.L., Sharp, W.D., Zhang, P.Z., 2006. East Asian summer monsoon variability during Marine Isotope Stage 5 based on speleothem delta O-18 records from Wanxiang Cave, central China. *Palaeogeography Palaeoclimatology Palaeoecology* 236, 5-19.

Key, C.H. and N.C. Benson. 2006. Landscape Assessment: Ground measure of severity, the Composite Burn Index; and Remote sensing of severity, the Normalized Burn Ratio. In D.C. Lutes; R.E. Keane; J.F. Caratti; C.H. Key; N.C. Benson; S. Sutherland; and L.J. Gangi. 2006. FIREMON: Fire Effects Monitoring and Inventory System. USDA Forest Service, Rocky Mountain Research Station, Ogden, UT. Gen. Tech. Rep. RMRS-GTR-164-CD: LA 1-51

Lloyd, R.M., 1967. Oxygen-18 composition of oceanic sulphate. *Science* 156, 1228–1231.

MacFarlane, C., Bond, C., White, D.A., Grigg, A.H., Ogden, G.N. and Silberstein, R., 2010. Transpiration and hydraulic traits of old and regrowth eucalypt forest in southwestern Australia. *Forest Ecol Manag* 260, 96-105.

Mahmud, K., Mariethoz, G., Treble, P.C. and Baker, A., 2015a. Terrestrial LiDAR survey and morphological analysis to identify infiltration properties in the Tamala Limestone, Western Australia. *IEEE Journal of Selected Topics in Applied Earth Observations and Remote Sensing*.

Mahmud, K., Mariethoz, G., Baker, A., Treble, P.C., Markowska, M. and McGuire, E., 2015b.

Estimation of deep infiltration in unsaturated limestone environments using cave LiDAR and drip count data. *Hydrological and Earth System Sciences Discussions* 19, 1-35.

Mattey, D.P., Fairchild, I.J., Atkinson, T.C., Latin, J.-P., Ainsworth, M., Durell, R., 2010. Seasonal microclimate ocntrol of calcite fabrics, stable isotopes and trace elements in modern speleothem from St Michaels Cave, Gibraltar, In: Pedley, H.M., Rogerson, M. (Eds.), Tufas and Speleothems: unravelling the microbial and physical controls. The Geological Society of London, London, pp. 323-344.

McDonald, J., Drysdale, R., Hill, D., 2004. The 2002–2003 El Nin˜o recorded in Australian cave drip waters:Implications for reconstructing rainfall histories using stalagmites. *Geophysical Research Letters* 31.

McDonald, J., Drysdale, R., Hill, D., Chisari, R., Wong, H., 2007. The hydrochemical response of cave drip waters to sub-annual and inter-annual climate variability, Wombeyan Caves, SE Australia. *Chemical Geology* 244, 605-623.

McDonald, J., Drysdale, R.N., 2007. Hydrology of cave drip waters at varying bedrock depths from a karst system in southeastern Australia. *Hydrological Processes* 21, 1737-1748.

McGillen, M.R. and Fairchild, I.J. 2005 An experimental study of the controls on incongruent dissolution of $CaCO_3$ under analogue glacial conditions. *Journal of Glaciology*, 51, 383-390.

McMillan, E.A., Fairchild, I.J., Frisia, S., Borsato, A., McDermott, F., 2005. Annual trace element cycles in calcite-aragonite speleothems: evidence of drought in the western Mediterranean 1200-1100 yr BP. *Journal Of Quaternary Science* 20, 423-433.

Mengel, K., Kirkby, E.A., Kosegarten, H., Appel, T. (eds.), 2001. Principles of plant nutrition. Springer Science and Business Media.

Meyer, K.W., Feng, W.M., Breecker, D.O., Banner, J.L. and Guilfoyle, A. (2014) Interpretation of speleothem calcite delta C-13 variations: Evidence from monitoring soil CO2, drip water, and modern speleothem calcite in central Texas. *Geochim Cosmochim Ac* 142, 281-298.

Miorandi, R., Borsato, A., Frisia, S., Fairchild, I., Richter, D., 2010. Epikarst hydrology and implications for stalagmite capture of climate changes at Grotta di Ernesto (NE Italy): results from long-term monitoring. *Hydrological Processes* 34, 3101-3114.

Musgrove, M., Banner, J.L., 2004. Controls on the spatial and temporal variability of vadose dripwater geochemistry: Edwards Aquifer, central Texas. *Geochimica et Cosmochimica Acta* 68, 1007-1020.

O'Connell, A.M. (1985) Nutrient accessions to the forest floor in karri (*Eucalyptus diversicolor* F. Muell.) forests of varying age. *Forest Ecol Manag* 10, 283-296.

O'Connell, A.M. and Grove, T.S. (1996) Biomass production, nutrient uptake and nutrient cycling in the Jarrah (*Eucalyptus marginata*) and Karri (*Eucalyptus diversicolor*) forests of South-western Australia, in: M, A.P., A, A.M. (Eds.), Nutrition of Eucalypts. CSIRO Publishing, Melbourne, p. 440.

Orland, I.J., Burstyn, Y., Bar-Matthews, M., Kozdon, R., Ayalon, A., Matthews, A. and Valley, J.W. (2014) Seasonal climate signals (1990-2008) in a modern Soreq Cave stalagmite as revealed by high-resolution geochemical analysis. *Chem Geol* 363, 322-333.

Parkhurst D. L. and Appelo C. A. J. (1999) User's guide to PHREEQC (Version 2)—A computer program for speciation, reaction-path, 1D-transport, and inverse geochemical calculations. U.S. Geol. Surv. Water Resour. Inv. Rep. 99-4259.

Peck, A.J., Johnston, C.D., Williamson, D.R., 1981. Analyses of solute distributions in deeply weathered soils. *Agricultural Water Management* 4, 83-102.

Raupach, M.R., Briggs, P.R., Haverd, V., King, E.A., Paget, M, Trudinger, C.M., 2009. Australian Water Availability Project (AWAP): CSIRO Marine and Atmospheric Research Component: Final Report for Phase 3. CAWCR Technical Report No. 013. 67 pp.

Raupach, M.R., Briggs, P.R., Haverd, V., King, E.A., Paget, M, Trudinger, C.M., 2011. Australian Water Availability Project. CSIRO Marine and Atmospheric Research, Canberra, Australia. <http://www.csiro.au/awap>.

Rees, C.E., Jenkins, W.J., Monster, J., 1978. The sulphur isotopic composition of ocean water sulphate. *Geochim Cosmochim Acta* 42(4): 377–381.

Rutlidge, H., Baker, A., Marjo, C.E., Andersen, M.S., Graham, P., Cuthbert, M.O., Rau, G.C., Roshan, H., Markowska, M., Mariethoz, G., & Jex, C., 2014. Dripwater organic matter and trace element geochemistry in a semi-arid karst environment: implications for speleothem paleoclimatology. *Geochimica et Cosmochimica Acta.* Vol. 135, p. 217–230.

Sands, R. and Mulligan, D.R., 1990. Water and nutrient dynamics and tree growth. *Forest Ecology and Management* 30, 91-111.

Sinclair, D.J., Banner, J.L., Taylor, F.W., Partin, J., Jenson, J., Mylroie, J., Goddard, E., Quinn, T., Jocson, J., Miklavic, B., 2012. Magnesium and strontium systematics in tropical speleothems from the Western Pacific. *Chemical Geology* 294, 1-17.

Sundqvist, H.S., Holmgren, K., Fohlmeister, J., Zhang, Q., Bar Matthews, M., Spotl, C., Kornich, H., 2013. Evidence of a large cooling between 1690 and 1740 AD in southern Africa. *Scientific Reports* 3.

Tadros, C.V., Hughes, C.E., Crawford, J., Hollins, S.E. and Chisari, R. (2014) Tritium in Australian precipitation: A 50 year record. *J Hydrol* 513, 262-273.

Tooth, A.F., Fairchild, I.J., 2003. Soil and karst aquifer hydrological controls on the geochemical evolution of spleothem-forming drip waters, Crag Cave, southwest Ireland. *Journal of Hydrology* 273,

51-68.

Treble, P., Shelley, J.M.G., Chappell, J., 2003. Comparison of high resolution sub-annual records of trace elements in a modern (1911-1992) speleothem with instrumental climate data from southwest Australia. *Earth And Planetary Science Letters* 216, 141-153.

Treble, P.C., Bradley, C., Wood, A., Baker, A., Jex, C.N., Fairchild, I.J., Gagan, M.K., J, C., C, A., 2013. An isotopic and modelling study of flow paths and storage in Quaternary aeolinite, SW Australia: implications for speleothem paleoclimate records. *Quaternary Science Reviews* 64, 90-103.

Treble, P.C., Fairchild, I.J., Griffiths, A., Baker, A., Meredith, K.T., Wood, A. and McGuire, E. (2015) Impacts of cave air ventilation and in-cave prior calcite precipitation on Golgotha Cave dripwater chemistry, southwest Australia. *Quaternary Science Reviews* 127, 61-72.

Tremaine, D.M. and Froelich, P.N. (2013) Speleothem trace element signatures: A hydrologic geochemical study of modern cave dripwaters and farmed calcite. *Geochimica et Cosmochimica Acta* 121, 522-545.

Yusiharni, E. and Gilkes, R. (2012) Minerals in the ash of Australian native plants. *Geoderma*, 189-190, 369-380.

Wong, C.I., Banner, J.L. and Musgrove, M. (2011) Seasonal dripwater Mg/Ca and Sr/Ca variations driven by cave ventilation: Implications for and modeling of speleothem paleoclimate records. *Geochimica et Cosmochimica Acta* 75, 3514-3529.

Wynn, P.M., Fairchild, I.J., Baker, A., Baldini, J.U.L. and McDermott, F. (2008) Isotopic archives of sulphate in speleothems. *Geochimica et Cosmochimica Acta* 72, 2465-2477.

Wynn, P.M., Borsato, A., Baker, A., Frisia, S., Miorandi, R. & Fairchild, I.J. 2013 Biogeochemical cycling of sulphur in karst and transfer into speleothem archives at Grotta di Ernesto, Italy. *Biogeochemistry*, 114, 255-267.

Wynn, P.M., Fairchild, I.J., Frisia, S., Spotl, C., Baker, A. and Borsato, A., 2010. High-resolution sulphur isotope analysis of speleothem carbonate by secondary ionisation mass spectrometry. *Chemical Geology*, 271, 101 – 107.

Wynn, P.M., Loader, N. and Fairchild, I.J., 2014a. Interrogating trees for isotopic archives of atmospheric sulphur deposition and comparison to speleothem records. *Environmental Pollution*, 187, 98-105.

Wynn, P.M., Fairchild I.J., Spötl, C, Hartland, A., Mattey, D., Fayard, B., Cotte, M., 2014b. Synchrotron X-ray distinction of seasonal hydrological and temperature patterns in speleothem carbonate. *Environmental Chemistry*. 11, 28-36.